J. Phys.: Condens. Matter **20** (2008) 083203 (21pp) doi:10.1088/0953-8984/20/8/083203

TOPICAL REVIEW

Density functional calculations of nanoscale conductance

Max Koentopp[1], **Connie Chang**[1], **Kieron Burke**[2] **and Roberto Car**[3]

[1] Department of Chemistry and Chemical Biology, Rutgers University, 610 Taylor Road, Piscataway, NJ 08854, USA
[2] Department of Chemistry, UC Irvine, 1102 Natural Sciences 2, Irvine, CA 92697, USA
[3] Department of Chemistry and Princeton Institute for the Science and Technology of Materials (PRISM), Princeton University, Princeton, NJ 08544, USA

Received 28 March 2007, in final form 14 November 2007
Published 1 February 2008
Online at stacks.iop.org/JPhysCM/20/083203

Abstract
Density functional calculations for the electronic conductance of single molecules are now common. We examine the methodology from a rigorous point of view, discussing where it can be expected to work, and where it should fail. When molecules are weakly coupled to leads, local and gradient-corrected approximations fail, as the Kohn–Sham levels are misaligned. In the weak bias regime, exchange–correlation corrections to the current are missed by the standard methodology. For finite bias, a new methodology for performing calculations can be rigorously derived using an extension of time-dependent current density functional theory from the Schrödinger equation to a master equation.

(Some figures in this article are in colour only in the electronic version)

Contents

1. Introduction and notation

Single molecules used as building blocks such as diodes, transistors, or switches have attracted much interest as a basis for a future *molecular electronics* [1]. Many groups worldwide have been performing either experiments or calculations. There has been tremendous progress, especially in the areas of metallic wires [2–6] and nanotubes [7–13]. However, comparison between theory and experiment has been much less successful for molecular electronics, i.e., organic molecules between two electrodes. Experimentally, obtaining consistently reproducible results from device to device has been problematic [14, 15]. Theoretically, the challenge is finding a method to quantitatively determine device characteristics with neither empirical input nor over-parametrization [16, 17, 19, 20].

In recent years, density functional theory (DFT) calculations of electronic transport through single molecules have been published by an ever increasing number of research groups. We focus here on purely electronic transport

 © 2008 IOP Publishing Ltd Printed in the UK

calculated with DFT based methods. The most prominent method is the Landauer-type scattering formalism [21–24], formulated in terms of Green's functions in combination with ground-state DFT. It can be derived using the Keldysh non-equilibrium Green's function formalism [25, 27]. In the following, we will call this method *the standard approach*. It can also be obtained from elementary scattering theory (e.g. [17, 26]), or using the Kubo linear response formula [28, 29, 111]. However, such derivations are limited to at best Hartree-interacting electrons, as we discuss. Apart from calculating the current–voltage characteristics of a coherent molecular junction in the Landauer scattering picture [17, 26, 27, 30–33, 35–40], several additional aspects such as electron–phonon coupling [41, 52, 53], conformation-induced switching [54–58], or interaction with light [55] have also been addressed within these methods. Questions discussed also include the influence of electrode–molecule bond geometry [17, 30, 59–62] or effects of a gate electrode [19, 42, 58, 63].

Whereas ground-state DFT has become quite reliable for calculating the electronic structure and other properties of molecules and solids [64], this success has not extended to transport calculations through organic molecules [17, 19]. While these calculations were originally greeted with much enthusiasm, researchers in the many-body community have always been sceptical [65–67]. A simple question to ask is, can such calculations correctly describe the Coulomb blockade regime? That the answer is patently no has raised doubts about the validity of this approach among that community. These doubts have been further compounded by the fact that calculations within this scattering framework usually overestimate the experimentally measured conductance of organic molecules by about one order of magnitude [17, 19]. Only for transport through atomic metallic wires [2–5], do calculations yield results in agreement with experiment, but this is not a true test of the method, as the same result is found in any calculation yielding a unit of conductance per channel.

The performance of this standard approach is the main subject of this review. As we describe below, neither of the traditional tests of DFT calculations, i.e., direct comparison with experiment or benchmark testing against more accurate theoretical methods for smaller systems, are generally available for this problem. On the one hand, the experimental situation is often not well characterized, while on the other, these are transport calculations with systems of up to several hundred atoms. Alternative treatments are either prohibitively expensive or of such a modelistic nature as to not allow meaningful tests. Thus, at present, there is no simple way to know when the standard approach is accurate or reliable. Instead, we examine carefully DFT treatments, and show that the standard approach is an approximation to a more general approach using time-dependent DFT, and from this perspective, its limitations can be deduced.

Ground-state DFT is based on rigorous theorems and so, if correctly applied to a problem, using a sufficiently accurate approximate functional, will produce an accurate result. The purpose of the present article is to ask two simple questions: (a) is the present *standard approach* formulation derivable from the basic theorems of ground-state DFT, and (b) if so, are our present approximations sufficiently accurate for conductance calculations? The answers show a variety of deficiencies (e.g. inadequacy of the ground-state approximation, approximations made by using local functionals) in the present theory and we do not yet know how important these drawbacks are. We do not know how frequently situations are encountered in which these limitations are quantitatively significant.

We discuss here three major issues that need to be resolved to improve on the present state of transport calculations. (i) The first involves the accuracy of ground-state functionals. The functionals presently used in the Landauer and Kohn–Sham approximations might not capture enough of the physics to be useful and more importantly they might not give good qualitative or quantitatively accurate results. The worst defect we have found is due to lack of derivative discontinuity in LDA and GGA functionals, which leads to an artificial level broadening and can greatly overestimate the conductance [19], due to incorrect positions of the resonances if the molecule is weakly coupled to the leads [68, 79]. (ii) The second issue is the missing exchange–correlation (XC) contribution in the Landauer formula. Present calculations entirely miss this contribution to the current. Some groups have sought to improve on the issues delineated in (i) and (ii) by calculating the XC corrections to the current via the gradient expansion corrections in the Vignale–Kohn approximation [20] and the exact exchange Kohn–Sham potential with the optimized effective potential (OEP) [79]. The exact exchange potential can also be estimated with self-interaction corrections (SIC) [68, 69] where the self-interaction errors in LDA DFT calculations are subtracted out. Furthermore, in the weak bias limit, a careful application of the Kubo response equation coupled with the DFT formulation, can be used to find the exact answer [19]. (iii) The third issue we address is an exact theory for finite bias, since transport experiments are often conducted under a finite voltage drop. Thus, an exact formula couched in DFT terms must be derived for these conditions.

In the last few years, the DFT computational transport community has become aware of these issues [17, 19, 20, 68], and a variety of approaches to overcome them have been suggested. Many are looking to alternative formulations, such as configuration–interaction (CI) in quantum chemistry [70] or GW in many-body physics [71, 72], to include effects that are missed in present (*standard approach*) DFT treatments. Such calculations are sorely needed, to test the DFT formulations against and learn their limitations. Accurate wavefunction treatments are extensively used in both ground-state DFT and TDDFT as benchmarks and to provide insight into functional development [73]. But since such calculations are typically far more expensive than DFT calculations, and given the chemical complexity of the devices that can be built, there remains an overriding need to develop a reliable DFT approach.

Thus a variety of new DFT based formulations of the problem are being developed. One discussed here includes using a Kohn–Sham effective single-particle version of a master equation formulation of transport [74] which will be discussed in section 5.1.2. Using TDDFT, another approach

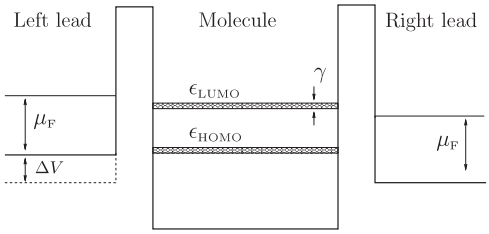

Figure 1. Schematic diagram of the potential of a resonant tunnelling device with the LUMO level of the device molecule sandwiched between the Fermi levels of the leads which are shifted relative to each other by an applied bias voltage ΔV. When $\Delta V = 0$, the chemical potential is $\mu_{\rm F}$. The LUMO and HOMO levels have a small width γ, indicating weak coupling to the leads.

obtains the current by calculating the time evolution of a system consisting of a molecule coupled to two finite metallic contacts and turning on a potential step, resulting in two different chemical potentials [75, 76]. A third is to use large finite leads, and watch a capacitance discharge [78]. All three methods essentially begin from a static distribution, apply some change, and allow the system to evolve to a steady, but non-equilibrium distribution. For non-interacting electrons in the weak bias limit, all agree, both with each other and the standard approach, but likely disagree in the general case of interacting electrons in finite bias. Under certain limiting conditions, such as adiabatic approximations to TDDFT, and local approximations to ground-state DFT, they yield the same results.

Because of the breadth of topics we cover in this review, we have collected the notation used in various formulae and expressions in table 1 for easy reference. We use atomic units ($e^2 = \hbar = m = 1$) throughout, unless otherwise stated. So all energies are in Hartree (1 H = 27.2 eV = 627 kcal mol^{-1}) and distances in Bohr radii (0.529 Å).

2. Review of the standard approach

In this section, we first review standard calculations that utilize a combination of ground-state DFT and the Landauer scattering formulation (the *standard approach*). We then look at approximations commonly employed in the course of calculating the conductance with this method.

2.1. Landauer scattering formulation

The Landauer scattering formulation can be easily understood in terms of a simple schematic form for a molecular tunnelling device, as shown in figure 1. In this cartoon, the electrons are non-interacting and the system is one dimensional. The leads are featureless boxes, and the 'molecule' consists of states localized to the barrier region. In the cartoon, $\mu_{\rm F}$ is the chemical potential of the entire system, i.e., in its ground state and in the absence of a bias. The molecule has been drawn so as to be weakly coupled to the leads, so that the levels on the molecule are only slightly broadened into resonances of width γ.

Table 1. Notation for formulae.

Symbol	Description
$n(\mathbf{r})$	electron density as a function of position
$v_{\rm ext}(\mathbf{r})$	ext. potential due to nuclei and ext. fields
$v_{\rm XC}(\mathbf{r})$	exchange–correlation potential
$v_{\rm H}(\mathbf{r})$	Hartree potential
$v_{\rm tot}(\mathbf{r})$	$v_{\rm ext}(\mathbf{r}) + v_{\rm H}(\mathbf{r})$, total electrostatic potential
$v_{\rm S}(\mathbf{r})$	KS potential= $v_{\rm ext}(\mathbf{r}) + v_{\rm H}(\mathbf{r}) + v_{\rm XC}(\mathbf{r})$
$\chi_{\rm S}(\mathbf{r}, \mathbf{r}', \omega)$	KS density–density response function
$\chi_{\rm prop}(\mathbf{r}, \mathbf{r}', \omega)$	proper susceptibility (density–density response function)
$\chi(\mathbf{r}, \mathbf{r}', \omega)$	many-body density–density response function
i	occupied level index
a	unoccupied level index
q	transition index of transition $i \rightarrow a$
$\Phi_q(\mathbf{r})$	$\Phi_i^*(\mathbf{r})\Phi_a(\mathbf{r})$ = KS ground-state orbitals
ω_q	$\epsilon_a - \epsilon_i$
$\alpha = {\rm L/R}$	quantum numbers for (left/right) lead electrons
i, j	indices for KS orbitals of the device region
α, β	Cartesian indices
$\epsilon_{k\alpha}$	energy of electron in lead $\alpha = {\rm L/R}$ with momentum k
$V_{k\alpha,n}$	coupling between leads and molecule
$c_{k\alpha}^\dagger (c_{k\alpha})$	creation (destruction) operator for electron with momentum k in lead α
$d_n^\dagger (d_n)$	creation (destruction) operator for electron with quantum numbers n on the molecule
$\rho_\alpha(\epsilon)$	density of states in lead α
$f_{\rm l/R}(\epsilon)$	Fermi–Dirac distribution functions in leads
$\Gamma_{i,j}^{\rm L/R}$	transition rate to left(right) lead $= 2\pi \sum_{\alpha\epsilon{\rm L/R}} \rho_\alpha(\epsilon) V_{\alpha,i}(\epsilon) V_{\alpha,j}^*(\epsilon)$
$\mathbf{g}^r$	surface Green's function for the leads
$\boldsymbol{\tau}$	hopping matrix describing the coupling between leads and molecule, its elements are given by $V_{k\alpha,n}$
$\sum_{\rm R}(\sum_{\rm L})$	self-energy matrices $= \boldsymbol{\tau}\mathbf{g}^r\boldsymbol{\tau}^\dagger$
$\mathbf{G}^{a(r,>,<)}$	full advanced (retarded, greater, lesser) Green's function for the extended molecule
$\mathbf{g}_0$	unperturbed KS Green's function for device
$\Psi_{\rm S}$	TDDFT KS wavefunction of the entire system
Ψ_α	TDDFT KS wavefunction projected on the leads $\alpha = {\rm L, R}$
$\Psi_{\rm C}$	TDDFT KS wavefunction projected on the central (molecule) region
$H_{\alpha\beta}$	block of the TDDFT KS Hamiltonian with $\alpha, \beta = {\rm L(left), R(right), C(centre/molecule)}$
$\epsilon_{\rm res}$	position of level in a resonant tunnelling device
γ	width of resonance in a resonant tunnelling device/coupling to the leads
$T(\epsilon)$	transmission coefficient as a function of energy
$n(\epsilon)$	spectral density of states
f	occupation of level
$\epsilon_{\rm F}$	Fermi energy
$\epsilon_{\rm HOMO}(\epsilon_{\rm LUMO})$	HOMO (LUMO) level of device
$\sigma(\mathbf{r}, \mathbf{r}', \omega)$	conductivity (current–current response function)
$S_{\rm T}$	density matrix for total system
S	reduced density matrix

In the Landauer picture, the applied bias raises the potential on the left lead by an amount ΔV. There is now an imbalance in the system. If one waits a long enough time,

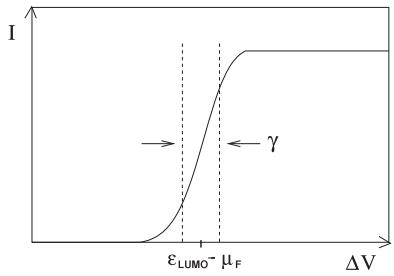

Figure 2. Schematic current–voltage characteristic of the resonant tunnelling device displayed in figure 1. The onset of the current occurs around $\epsilon\text{LUMO} - \mu_\text{F}$. The step is broadened by the coupling γ.

eventually many electrons would flow from the left to the right, and re-establish equilibrium, with a common chemical potential. This is not the regime we are interested in. Instead, on an intermediate timescale, one assumes a steady current is established, that is sufficiently small as to have no effect on the reservoir levels.

The current can then be calculated from the two-terminal Landauer formula [21] which, for this case, is simply

$$I = \frac{2}{\pi}\int_{-\infty}^{\infty} \mathrm{d}\epsilon \Delta f\, T(\epsilon) \tag{1}$$

where

$$\begin{aligned}\Delta f &= f_\text{L}(\epsilon) - f_\text{R}(\epsilon)\\ &= f(\epsilon - \mu_\text{F} - \Delta V) - f(\epsilon - \mu_\text{F})\end{aligned} \tag{2}$$

and $T(\epsilon)$ is the transmission coefficient at energy ϵ. The factor of two is for the two spin channels.

This can be easily understood as follows. Considered as a function of energy, only those states in the window between μ_F and $\mu_\text{F} + \Delta V$ can carry a net current. Those below are occupied on both sides, those above are unoccupied on both sides. Each state of energy ϵ in the window will transmit an electron with probability $T(\epsilon)$, yielding that contribution to the net current. The schematic diagram shown in figure 1 will yield a current bias curve like that shown in figure 2. The differential conductance, $\mathrm{d}I/\mathrm{d}\Delta V$, will be strongly peaked in the position of the LUMO. The result is even simpler in the zero bias limit, as $\mathrm{d}V \to 0$. Then, $\mathrm{d}f = \delta(\mu_\text{F})\,\mathrm{d}V$, so that the conductance becomes

$$G = \frac{\mathrm{d}I}{\mathrm{d}V} = \frac{2T(\mu_\text{F})}{\pi}. \tag{3}$$

Thus for non-interacting electrons in a fixed potential, the Landauer formula is easily understood and justified.

2.2. Interacting electrons

The Landauer formula for non-interacting (or at most Hartree-interacting) electrons was later generalized to interacting electrons by Meir and Wingreen [25], who formulated an algorithm for calculating the current using the full non-equilibrium Green's functions for the system. They employ a second quantized Hamiltonian description for the electrons in the leads, the interacting region (molecule), and the coupling between them. Initially uncoupled, the coupling between the leads and the molecule is turned on slowly via the $V_{ka,n}$ term in equation (4):

$$\begin{aligned}H = &\sum_{k,a\,\epsilon\,\text{L,R}} \epsilon_{ka} c^\dagger_{ka} c_{ka} + H_\text{int}(\{d^\dagger_n\};\{d_n\})\\ &+ \sum_{k,a\,\epsilon\,\text{L,R}} (V_{ka,n} c^\dagger_{ka} d_n + \text{H.c.}).\end{aligned} \tag{4}$$

Here, k refers to the momentum of an electron with energy ϵ_{ka} in the left or right lead, labelled by α. The creation and annihilation operators are denoted by $c^\dagger(c)$ and $d^\dagger(d)$, referring to the leads and the molecule, respectively. Then, using the continuity equation for the current, the Keldysh formalism for the Green's functions and allowing the electrons in the device region to interact while keeping the electrons in the leads non-interacting, they find an expression for the current when the leads are at different chemical potentials:

$$\begin{aligned}I = \frac{2}{\pi}\int \mathrm{d}\epsilon (&\mathrm{tr}\{[f_\text{L}(\epsilon)\Gamma^\text{L}_{i,j} - f_\text{R}(\epsilon)\Gamma^\text{R}_{i,j}](G^r_{i,j} - G^a_{i,j})\}\\ &+ \mathrm{tr}\{(\Gamma^\text{L}_{i,j} - \Gamma^\text{R}_{i,j})G^<_{i,j}\}),\end{aligned} \tag{5}$$

and $\Gamma^{\text{L/R}}_{i,j} = 2\pi \sum_{a\,\epsilon\,\text{L/R}} \rho_a(\epsilon) V_{a,i}(\epsilon) V^*_{a,j}(\epsilon)$ where i, j indexes the states in the interacting region and a indexes the states in the leads. $\mathbf{G}^r$, $\mathbf{G}^a$, and $\mathbf{G}^<$ refer respectively to the retarded, advanced, and lesser Green's functions. Meir and Wingreen [25] derived a simpler formula for the case of proportional couplings ($\Gamma^\text{R}_{i,j} = \alpha\Gamma^\text{L}_{i,j}$)

$$I = \frac{2}{\pi}\int \mathrm{d}\epsilon \left[f_\text{L}(\epsilon) - f_\text{R}(\epsilon)\right] \mathrm{Im}\left[\mathrm{tr}\left\{\mathbf{\Gamma G}^r\right\}\right], \tag{6}$$

where $\mathbf{\Gamma} = \mathbf{\Gamma}^\text{L}\mathbf{\Gamma}^\text{R}/(\mathbf{\Gamma}^\text{L} + \mathbf{\Gamma}^\text{R})$. This however, is a strong limitation due to their reliance on symmetric contacts which is never fulfilled for a realistic system. Only an atomic point contact could satisfy this condition since it requires that each orbital on the device couples equally to the left and right contact. This restriction can be removed [17, 75], resulting in a general formula for the current in terms of the non-equilibrium, self-consistent Green's function.

2.3. The standard approach

Because of the difficulties involved in solving the full many-body problem for the non-equilibrium Green's functions exactly for an interacting system of many electrons, the Green's function in equation (5) is usually approximated with the ground-state Kohn–Sham effective single-particle Green's function (DFT–NEGF). This complicates the simple picture of figure 1 somewhat, as the KS potential changes with the applied bias. A self-consistent KS potential must be found, which will continuously change from being raised by ΔV on the left, to being at its equilibrium level on the right. These changes will not be confined solely to the molecule, but should die off within one or two Fermi wavelengths into the leads. Thus one must define an extended molecule as in figure 3, which includes those parts of the leads where the KS potential differs from its non-biased value.

Also note that in most calculations, the molecule is chemically bonded to the leads. Thus its levels will be much

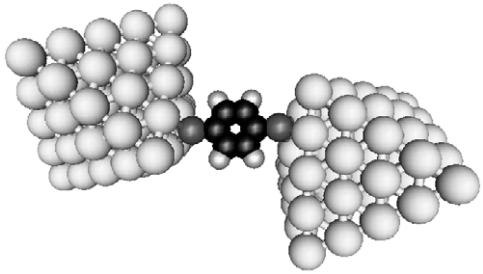

Figure 3. Landauer approach: schematic representation of a benzene-1,4-dithiol molecule between two gold contacts. The molecule plus gold pyramids (55 atoms each) constitute the *extended molecule* as used in the DFT calculations for the *standard approach*.

broader than pictured in figure 1, overlapping with one another, and delocalizing into the leads.

In addition, approximations to the self-energy matrix $\mathbf{\Sigma}_{\mathrm{R}}$ and $\mathbf{\Sigma}_{\mathrm{L}}$ are made (e.g. [26, 30, 32]). The coupling between the right lead and the device is described by the hopping matrix $\boldsymbol{\tau}_{\mathrm{R}}$ (whose elements are just the coupling terms $V_{ka,n}$ in equation (4)) and similarly for the coupling between the left lead and the device. There is no direct coupling between the leads as this would cause electrons from the left lead to run into the right lead until a global equilibrium was reached. Then, the self-energy that encapsulates the effects of coupling the left contact to the device can be written as:

$$\mathbf{\Sigma}_{\mathrm{L}} = \boldsymbol{\tau}_{\mathrm{L}} \mathbf{g}_{\mathrm{L}}^{r} \boldsymbol{\tau}_{\mathrm{L}}^{\dagger} \tag{7}$$

where $\mathbf{g}_{\mathrm{L}}^{\mathrm{R}}$ is the surface Green's function for the left lead. An equivalent expression can be derived for the right contact. The full Green's function for the device region, $\mathbf{G}$, can then be written in terms of the unperturbed KS Green's function, $\mathbf{g}_0^r$, for the extended molecule (molecule plus small parts of the leads, figure 3) as

$$\mathbf{G}^{-1} = \mathbf{g}_0^{-1} + \mathbf{\Sigma}_{\mathrm{L}} + \mathbf{\Sigma}_{\mathrm{R}}. \tag{8}$$

The coupling matrices $\mathbf{\Gamma}^{R(L)}$ are given in terms of the self-energy matrices as

$$\mathbf{\Gamma}^{\mathrm{L(R)}} = -\mathrm{i}(\mathbf{\Sigma}_{\mathrm{L(R)}} - \mathbf{\Sigma}_{\mathrm{L(R)}}^{\dagger}) = 2\,\mathrm{Im}\,\mathbf{\Sigma}_{\mathrm{L(R)}}. \tag{9}$$

This self-energy only describes hopping onto and off the device from the leads, but neglects the other processes that can occur in the leads. The leads are thus assumed to be non-interacting. In this situation, a Dyson equation for the device region leads to the formula for the current for the case of non-interacting electrons derived from the more general expression given in equation (5):

$$I = \frac{2}{\pi} \int \mathrm{d}\epsilon \left[f_{\mathrm{L}}(\epsilon) - f_{\mathrm{R}}(\epsilon) \right] \mathrm{tr} \left\{ \mathbf{G}^{a} \mathbf{\Gamma}^{\mathrm{R}} \mathbf{G}^{r} \mathbf{\Gamma}^{\mathrm{L}} \right\}. \tag{10}$$

Identifying the trace with a transmission coefficient, this is identical to equation (1). This approach has been implemented successfully by many groups by now (e.g. [18, 26, 27, 30–35, 37–40, 49, 80]), and calculations have been performed for a large variety of molecules, coupled to electrodes of different materials like gold, platinum and silicon. Molecules studied vary from H_2 to alkyl chains, to molecules built from aromatic subunits, or metallo-organic complexes. With successful we refer to a calculation in which the described standard formalism has been implemented and applied in a correct way. Especially early DFT based calculations of molecular conductance often had some shortcomings in the implementation or application, e.g. the coupling to the macroscopic leads was not accounted for in an appropriate way, which lead to strong deviations in the calculated current. Successful implementations, when applied to the same molecular system and contact geometry with the same functional performed by different groups yield similar results. However, the calculated conductances usually overestimate the experimentally measured ones by about one order of magnitude [17, 19]. By far the best studied molecule is benzenedithiol coupled to gold contacts via the sulfur atoms [17, 32, 34, 40, 42–50, 59]. Figure 9 shows results from a calculation [19] using the geometry in figure 3 and comparing DFT with HF. Other calculations use slightly different geometries, like e.g. planar gold surfaces and a super cell. Using the latter geometry, calculations [51] employing the master equation approach yield a zero bias conductance of $\approx 0.4 G_0$, in very good agreement with Transiesta calculations [34] ($\approx 0.4 G_0$) and the results in figure 9 ($0.3 G_0$), which both employed slightly different geometries.

2.4. Limitations of the standard approach

Transport is inherently a time-dependent non-equilibrium problem with current flow which is not at all within the domain of validity of a ground-state DFT description. Its natural description is found within time-dependent (current) DFT. Therefore, using ground-state DFT to calculate the device Green's function incorporates several uncontrolled approximations and errors which will be investigated in sections 3 and 4. The time-dependent (TD) XC potential can be very different from its ground-state counterpart. First, the step from time-dependent DFT to ground-state DFT misses all dynamic effects, i.e., the adiabatic approximation of section 4.2. Also, for example, the partitioned system is assumed to be in equilibrium and disconnected from the leads at some initial time. Slowly, a finite voltage is turned on which shifts the chemical potentials of the leads. This necessarily drives the system out of equilibrium and so the electron distribution in the leads do not follow the equilibrium Fermi distributions. This effect is probably small, but its presence points to the many problems with this approach.

Other problems with this approach include the incorrect placement of energy levels due to the missing derivative discontinuity when a local approximation to the XC functional is employed. This leads to an error in the location of the resonance peaks (section 3). The failure of local functionals to reproduce the derivative discontinuity also produces resonance peaks that are too wide in energy which results in a general overestimation of the conductance.

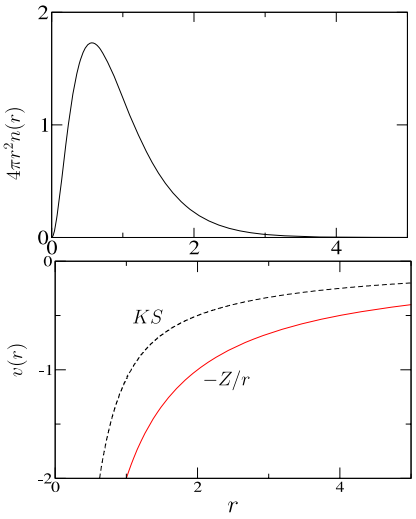

Figure 4. Top panel—exact radial density for the He atom. Bottom panel—external and exact KS potentials for the He atom (atomic units).

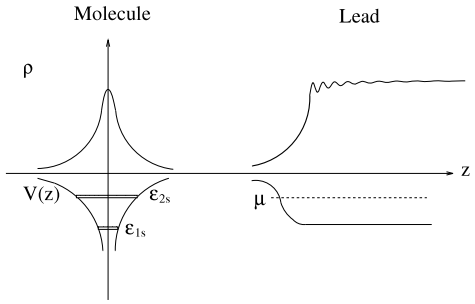

Figure 5. Density and potential of a molecule–lead system where resonance occurs when the chemical potential of the lead lines up with ϵ_{LUMO} of the molecule.

Table 2. Exact Kohn–Sham energies for the He atom, i.e. the orbitals for the KS potential of figure 4.

Orbital	Energy (H)
1s	−0.903 724 36
2s	−0.157 731 64
2p	−0.126 569 95
3s	−0.064 547 05

3. Inadequacy of ground-state approximations

In this section, we take the *standard approach* prescription at face value, and assume it would give the correct conductance if implemented with the exact ground-state density functional. (In the next sections, we will show that this is unlikely to be true in general.) But we ask the simple question: using present standard density functional approximations (LDA, GGA, hybrids), will we get accurate results? To answer this question, we must first review some facts that are well known in the DFT community.

3.1. Exact ground-state DFT

In the top panel of figure 4 we show the exact density $n(\mathbf{r})$ of the He atom, calculated by Umrigar *et al* [81], using quantum Monte Carlo to minimize the energy of a highly accurate wavefunction. In the bottom panel of figure 4 we plot both the nuclear (i.e. external potential) potential, which is $-Z/r$ in atomic units, and the exact Kohn–Sham potential $v_{\mathrm{S}}(\mathbf{r})$ for this system. Two non-interacting electrons, inserted in this potential, reproduce *exactly* the density of the top panel of figure 4. By the Hohenberg–Kohn theorem [82], this potential (if it exists) is unique. All modern Kohn–Sham density functional calculations [83] are calculations of these fictitious non-interacting electrons in a KS potential. The goal of much research in DFT is to provide ever more reliable approximations to the exchange–correlation (XC) energy, $E_{\mathrm{XC}}[n]$. Its functional derivative with respect to density provides the Kohn–Sham potential via

$$v_{\mathrm{S}}(\mathbf{r}) = v_{\mathrm{ext}}(\mathbf{r}) + v_{\mathrm{H}}(\mathbf{r}) + v_{\mathrm{XC}}(\mathbf{r}), \tag{11}$$

where $v_{\mathrm{ext}}(\mathbf{r})$ is the original external potential, $v_{\mathrm{H}}(\mathbf{r})$ is the Hartree (or classical or electrostatic) potential, and $v_{\mathrm{XC}}[n](\mathbf{r}) = \delta E_{\mathrm{XC}}[n]/\delta n(\mathbf{r})$ is the XC potential. In traditional ground-state DFT, the eigenvalues of the KS potential, ϵ_i, have no formal meaning, except that the eigenvalue of the highest occupied molecular orbital (HOMO) is exactly the negative of the ionization energy (Koopmans' theorem), as can be shown by studying the asymptotic decay of the density [84]. However, the lowest unoccupied molecular orbital (LUMO) eigenvalue does not in general match the negative of the electron affinity, i.e.,

$$\epsilon_{\mathrm{HOMO}} = -I, \qquad \epsilon_{\mathrm{LUMO}} \neq -A. \tag{12}$$

In He, $\epsilon_{1\mathrm{s}} = \epsilon_{\mathrm{HOMO}} = -0.903$ H, but $\epsilon 2\mathrm{s} = \epsilon_{\mathrm{LUMO}} = -0.158$ H, while the electron affinity $A = 0$. Thus the fundamental gap, $I - A$, is not equal to the KS gap, i.e., the HOMO–LUMO energy difference, see table 2.

What happens then, as electrons are added to the system? This question was answered more than 20 years ago. Consider a hydrogen atom, far (say 10 Å) from a featureless metal surface (e.g., jellium), as shown in figure 5, and ask what happens to the KS potential as a function of the global chemical potential of the system. Since we chose the H atom far from the surface, its energy levels pick up a tiny width γ, as they are broadened into resonances. If μ matches the LUMO energy, as shown in the cartoon, electrons would occupy that level. But as soon as there is even an infinitesimal occupation, the level must move, in such a way as to keep the exact Koopmans' theorem satisfied. Since the density changes at most infinitesimally, the only allowed change (in the region of the atom) is a constant jump in the KS potential, by exactly the amount needed to restore Koopmans' theorem for the new HOMO. This is shown in figure 6.

3.2. DFT approximations

The success of most DFT calculations is based on good approximations to the XC energy itself, as this determines

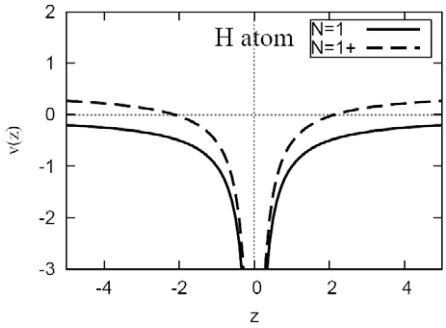

Figure 6. Exact KS potentials for H and H with an extra infinitesimal electron, illustrating the derivative discontinuity.

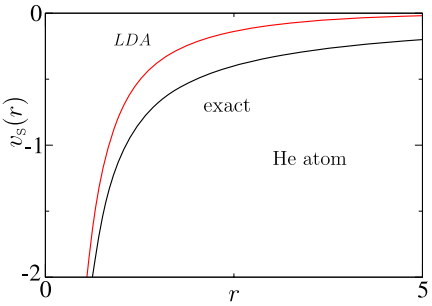

Figure 7. Exact and LDA KS potentials for the He atom.

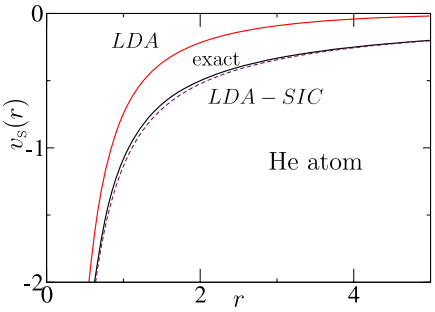

Figure 8. Perdew Zunger self-interaction corrected KS potential for He (dashed line). Exact and LDA KS potentials for the He atom for comparison.

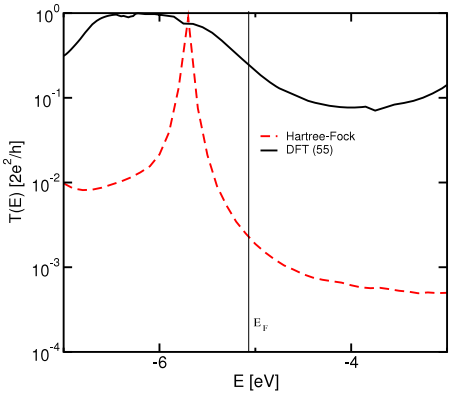

Figure 9. Transmission coefficient over energy for benzene-1,4-dithiol using DFT in the *standard approach* within a semi-local approximation (GGA) (solid line) compared with HF results (dashed line). Fermi energy is ≈−5.1 eV [17].

so many properties of the system. The most popular approximations, such as LDA [83], GGA [85], and hybrids of exact exchange and GGA, such as B3LYP [86] and PBE0 [87], have well known successes and failures. But they have the following failures in common, because they are *density* functionals:

- Self-interaction error: none are exact for a one-electron system, in which

$$E_X = -U, \qquad E_C = 0 \quad (1 \text{ electron}). \tag{13}$$

- They all have poorly behaving potentials far from the nuclei. The true KS potential decays as $-1/r$ far from a neutral atom, and this contribution is from the exchange potential. In figure 7, we have also plotted the LDA potential for the He atom. It decays far too rapidly, and so its orbitals are far too shallow. The HOMO is at -0.5704 H, while the LUMO is not bound at all.
- None contain the derivative discontinuity, so their potentials do not jump when the particle number passes through an integer.

(Actually, hybrids have about 1/4 exact exchange, but this is not enough to cure these ills.)

On the other hand, *orbital*-dependent functionals cure all these ills (at least, approximately). The original and simplest method is the self-interaction correction of Perdew and Zunger [88], and is often used with LDA for strongly correlated systems. The corrected exchange–correlation term is then given by:

$$E_{XC}^{LDA-SIC}[n] = E_{XC}^{LDA}[n] - \sum_i (E_H[n_i] + E_{XC}^{LDA}[n_i]), \tag{14}$$

where $n_i(r) = |\phi_i(\mathbf{r})|^2$. This functional is exact for one electron, decays correctly at large r, and its potential jumps discontinuously at integer particle number. The dashed line in figure 8 shows the huge improvement in the potential compared to LDA for the He case. More satisfactorily, there are now many implementations of exact exchange within DFT, in which the orbital-dependent exchange is treated as an implicit density functional [89]. Such optimized effective potential (OEP) calculations are often prohibitively expensive for large molecules, but are exact for one electron, have a potential that decays as $-1/r$, and $v_S(\mathbf{r})$ jumps discontinuously when a fraction of an electron is added.

Without some form of self-interaction correction, continuous density functionals allow electrons to self-repel, yielding orbitals that are too diffuse, in potentials that are too shallow.

3.3. Effect on transport

The missing orbital effects in approximate density functionals can have drastic consequences for calculations of conductances. For example, the missing derivative discontinuity in local approximations of DFT affects the magnitude of the conductance and misplaces the resonance peaks. This effect is strongest when the molecule is coupled weakly to the leads. For the exact Kohn–Sham potential as discussed above, the

potential is discontinuous, suddenly shifting by a constant while the energy remains continuous, as the next unoccupied level begins to be infinitesimally occupied (see figure 6). The origin of this discontinuity is due to the fact that $\epsilon_{\rm LUMO}$, the Kohn–Sham LUMO (lowest unoccupied molecular orbital) for the N-electron system is not the same as the Kohn–Sham HOMO (highest occupied molecular orbital) for the $N+1$-electron system, as seen in section 3.1. In local approximations such as LDA and GGA, the fractionally occupied level shifts and moves continuously to the position of the HOMO of the $N+1$ system as the next unoccupied level begins to be fractionally populated. The effects for transport calculation are broad resonance peaks in transmission which lead to finite conductance even at energies off resonance, yielding an overall increase in conductance that is unphysical.

This was first illustrated in [17], where Evers *et al* performed a test calculation on a realistic system, finding transmission coefficients for benzene-1,4-dithiol covalently coupled to two gold clusters using DFT with a GGA, and comparing to Hartree–Fock (HF) methods. The calculations were performed only at zero bias and the results for the transmission (found from the corresponding Green's functions) are shown in figure 9. The transmission coefficient at the Fermi energy is reduced by a factor of 100 in the HF calculation. This is likely due to the GGA orbitals being too diffuse, due to the self-interaction error.

A more serious problem is due to the incorrect positions of unoccupied levels. To probe an unoccupied resonance at zero bias, we can apply a gate voltage $V_{\rm g}$ to a double barrier resonant tunnelling device (DBRTS) perpendicular to the leads, shifting the LUMO down to the Fermi level $\epsilon_{\rm F}$ ($=\mu$ at $T=0$). In figure 1, this simply reduces all molecular levels by $V_{\rm g}$. As a level passes through $\epsilon_{\rm F}$ as a function of the gate voltage, there will be a peak in the conductance. When the resonance starts to overlap with $\epsilon_{\rm F}$, the exact KS ground-state potential in the region of the molecule will differ significantly from the off-resonant situation, as it depends on the occupation, i.e. it will jump discontinuously by the derivative discontinuity. This thereby greatly changes the transmission characteristics. The transmission peaks are *not* at the position of the unoccupied resonances of the ungated situation.

For any sharp resonance, the transmission coefficient is given by

$$T(\epsilon)=\frac{(\gamma/2)^2}{(\epsilon-\epsilon_{\rm res})^2+(\gamma/2)^2} \tag{15}$$

where $\epsilon_{\rm res}$ and γ are the position and width of the resonance. In any self-consistent KS treatment (including using the *exact* ground-state functional), $\epsilon_{\rm R}$ and γ depend on the ground-state density, and therefore on the partial occupation, $0\leqslant f\leqslant 1$, of the resonant level.

We will now use a simple model to show how the use of smooth, approximate density functionals produces completely erroneous transmissions (and hence conductances) as a function of $V_{\rm g}$ [19]. Defining the KS spectral function $A_{\rm s}(\epsilon)={\rm Im}({\rm tr}\mathbf{G}_{\rm s}(\epsilon))$ we can write expressions for the spectral density of states, $n(\epsilon)=A_{\rm s}/\pi$, as well as for the transmission $T_{\rm s}=\gamma A_{\rm s}/2$. This yields a simple linear relationship between $n(\epsilon)$ and the transmission of such a level, $n(\epsilon)=2\,T_{\rm s}(\epsilon)/(\gamma\pi)$. The self-consistent occupation f of the level is found from integrating over $n(\epsilon)$ as

$$f=\int_{-\infty}^{\epsilon_{\rm F}}{\rm d}\epsilon\; n(\epsilon)=\frac{1}{2}+\frac{1}{\pi}\tan^{-1}\left\{2\frac{\epsilon_{\rm F}-\epsilon_{\rm res}(f)}{\gamma(f)}\right\}. \tag{16}$$

The transmission can be obtained by inverting equation (16):

$$T^{-1}(\epsilon_{\rm F})=1+\tan^2\{\pi(f(\epsilon_{\rm F})-1/2)\}. \tag{17}$$

For simplicity, neglect any dependence of γ on occupation f, i.e., $\gamma(f)=\gamma_0$, as the actual dependence is expected to be weak and to have only little effect on the transmission peaks. The transmission can alternatively be expressed in terms of the gate voltage. Setting $\epsilon_{\rm F}=0$ for $V_{\rm g}=0$ and assuming a shift of the energy levels by $-V_{\rm g}$ due to the applied gate voltage (gate efficiency $=1$), we can replace $\epsilon_{\rm F}$ by $V_{\rm g}$ in equations (16) and (17), thus describing the transmission in terms of an applied gate voltage instead:

$$T^{-1}(V_{\rm g})=1+\tan^2\left\{\pi(f(V_{\rm g})-1/2)\right\}. \tag{18}$$

Any calculation that has a derivative discontinuity would give the solid line in figure 10. In this example $\Delta\epsilon=\epsilon_{\rm HOMO}(N+1)-\epsilon_{\rm LUMO}(N)$ is several eV. The narrow resonance (width $\gamma=0.1$) is positioned at the energy of $\epsilon_{\rm HOMO}(N+1)$. On the other hand, the dashed line is the result for a smooth, (semi-)local density functional. As the $N+1$ level gets fractionally filled, the resonance moves continuously from $\epsilon_{\rm LUMO}(N)$ to $\epsilon_{\rm HOMO}(N+1)$, resulting in a smearing out of the resonance width. It can be seen that the position of the resonance is displaced in this case. It is now centred in between the LUMO of the N-electron system and the HOMO of the $N+1$-electron system, assuming $\epsilon_{\rm res}=\epsilon_{\rm LUMO}+f\,\Delta\epsilon$ (i.e. a linear dependence of the potential on the occupation for the smooth functional). The resonance peak should be located at the *true* HOMO of the $N+1$-electron system (the solid line).

Even in the extreme limit of no width of the level ($\gamma\to 0$), the resonance in LDA remains broad. For weakly coupled leads where, at any occupation, $\gamma\ll\Delta\epsilon$, the Fermi level is pinned to the resonance ($\epsilon_{\rm res}(f)\to\epsilon_{\rm F}$) for $f\neq 0$ or 1. This

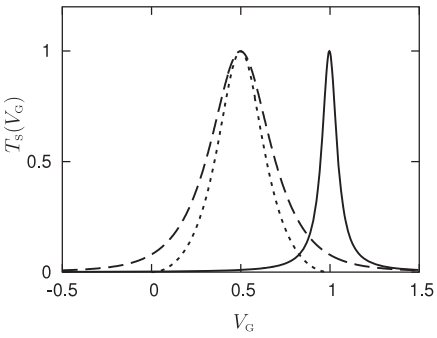

Figure 10. Double barrier resonant tunnelling system with a gate electrode. Zero bias transmission over gate voltage: dashed line is self-consistent approximate functional result, dotted line is approximate result for coupling $\gamma\to 0$, and solid line is exact result. Here $\epsilon_{\rm LUMO}(N)=0$, $\epsilon_{\rm HOMO}(N+1)=1$ and $\gamma_0=0.1$ [19].

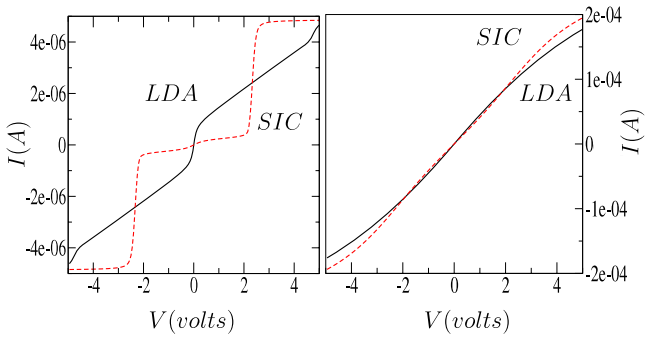

Figure 11. Current of a single energy level coupled to two metallic leads as a function of bias. Left figure corresponds to the case of weak coupling and right figure corresponds to the case of strong coupling. Solid lines are results for LDA and the dotted lines are results using self-interaction corrected LDA (LDA-SIC). From [68].

yields $\epsilon_{\rm F} = \epsilon_{\rm LUMO} + f\,\Delta\epsilon$ and using equation (17) we obtain the dotted line in figure 10. Thus, in a *standard* calculation using (semi)local functionals, equation (17) always produces a broad peak whose width is comparable to $\Delta\epsilon$, thereby overestimating the total conductance of the device—even when $\gamma \to 0$. For the case of a linear relation as discussed here, this artificial width is just $\Delta\epsilon/2$. In addition, the resonance position is incorrect, being $\Delta\epsilon/2$ too low.

It is possible to recover the derivative discontinuity and so avoid these artefacts with methods briefly described in section 3.2. The self-interaction is effectively removed either approximately from an LDA description via a self-interaction correction (LDA-SIC) or through the rather expensive, but more rigorous, OEP methods. In this method, the self-interaction can be removed explicitly, but it is computationally more feasible to parametrize the self-interaction in terms of its atomic components. What results is an orbital-dependent functional that incorporates non-local effects, yielding the derivative discontinuity.

Comparison of I–V curves between LDA and LDA-SIC was performed by Toher *et al* [68, 69] using a tight-binding calculation within the *standard approach*. The differences in the I–V characteristics were much less apparent for the case of strong coupling, confirming that the missing derivative discontinuity is most problematic in the limit of weak coupling. A cartoon of this effect can be seen in figure 11 where the current versus applied bias voltage of a device effective single-particle energy level is plotted for the LDA case (solid line), and the case for an artificial step-like energy (dotted line) which emulates the derivative discontinuity for the exact Kohn–Sham potential. The plot on the left-hand side reflects the situation of weak coupling to the leads ($\gamma = 0.2$ eV), whereas the plot on the right-hand side reflects the situation of strong coupling to the leads ($\gamma = 1.2$ eV).

4. Weak bias

In this section, we discuss—in the weak bias limit—the errors made due to the *standard approach* scheme. In this limit, we can use Kubo response theory to deduce the exact answer, and compare with the *standard approach*. We also give an estimate of the corrections in terms of the Vignale–Kohn current density functional. Local functionals not only miss the derivative discontinuity but also the XC contributions to the electric field response, which leads to an additional overestimation of the conductance. In the limit of low bias it is possible to describe transport with the Kubo response formulation. Seeing how the adiabatic local density approximation (ALDA) fails in this formulation provides clues as to the source of the problem and how to correct it. A more detailed discussion of calculations in this limit is given in section 5.1.1.

4.1. Time-dependent DFT

The usefulness of ground-state DFT has been augmented by the development and implementation of TDDFT [90]. The Runge–Gross theorem [91] shows that, under appropriate conditions, the time-dependent potential $v_{\rm ext}(\mathbf{r}, t)$ is a functional of the time-dependent density, $n(\mathbf{r}, t)$. This allows one to construct time-dependent Kohn–Sham equations, and use linear response theory to find TDDFT corrections to the KS transitions, making them the true excitations of the system.

How the linear response theory works can be seen in the density change to an applied perturbation varying as $\exp(\mathrm{i}\omega t)$, which can be expressed *exactly* in different ways:

$$\begin{aligned}\delta n(\mathbf{r}\omega) &= \int \mathrm{d}^3 r\, \chi(\mathbf{r}, \mathbf{r}', \omega)\, \delta v_{\rm ext}(\mathbf{r}, \omega) \qquad \text{(MB)}\\ &= \int \mathrm{d}^3 r\, \chi_{\rm prop}(\mathbf{r}, \mathbf{r}', \omega)\, \delta v_{\rm tot}(\mathbf{r}, \omega) \qquad \text{(EM)}\\ &= \int \mathrm{d}^3 r\, \chi_{\rm s}(\mathbf{r}, \mathbf{r}', \omega)\, \delta v_{\rm s}(\mathbf{r}, \omega) \qquad \text{(DFT)}\end{aligned}$$

where $v_{\rm tot}(\mathbf{r}\omega)$ is the sum of the external and induced (a.k.a. Hartree) potentials, while

$$\delta v_{\rm s}(\mathbf{r}, \omega) = \delta v_{\rm ext}(\mathbf{r}, \omega) + \delta v_{\rm H}(\mathbf{r}, \omega) + \delta v_{\rm XC}(\mathbf{r}, \omega) \qquad (19)$$

is the Kohn–Sham potential perturbation including the XC contribution. Different susceptibilities are used in different contexts: χ is the full many-body (MB) response function, giving the density change in response to the *external* perturbation; $\chi_{\rm prop}$ is the proper or irreducible susceptibility, giving the response to the perturbing potential of the total electric field, both external and induced (Hartree), used in electromagnetism (EM) [92]. Finally, $\chi_{\rm s}$ is the Kohn–Sham response function, constructed from KS energies and orbitals of the ground-state KS potential:

$$\chi_{\rm s}(\mathbf{r}\mathbf{r}'\omega) = 2\sum_q \frac{\Phi_q(\mathbf{r})\,\Phi_q^*(\mathbf{r}')}{\omega - \omega_q + \mathrm{i}0_+} + \text{c.c.}(\omega \to -\omega), \qquad (20)$$

and

$$\langle q|f|q'\rangle = \int \mathrm{d}^3 r \int \mathrm{d}^3 r'\, \Phi_q(\mathbf{r}) f(\mathbf{r}, \mathbf{r}') \Phi_{q'}(\mathbf{r}') \qquad (21)$$

where q is a double index, representing a transition from occupied KS orbital i to unoccupied KS orbital a, $\omega_q = \epsilon_a - \epsilon_i$, and $\Phi_q(\mathbf{r}) = \phi_i^*(\mathbf{r})\phi_a(\mathbf{r})$, where $\phi_i(\mathbf{r})$ is a KS orbital. Thus $\chi_{\rm s}$ is completely given by the ground-state KS calculation.

Table 3. Singlet transition energies for He, comparison of the true transitions with the Kohn–Sham transitions for the exact KS potential [96].

Transition	KS value (eV)[a]	True transition (eV)[b]
$1s \rightarrow 2p$	21.146	21.221
$1s \rightarrow 2s$	20.298	20.613
$1s \rightarrow 3s$	22.834	22.923

[a] The differences between the KS eigenvalues obtained using the exact potential [96].
[b] Accurate non-relativistic calculations from [97].

For example, it is the response of the two non-interacting KS electrons sitting in the KS potential of figure 2, and ω_q are the differences of the orbital energies listed in table 2. By definition, $\delta v_{\rm XC}(\mathbf{r}, \omega)$ causes these non-interacting electrons to have the same density response as the real electrons. Expanding this around the original ground-state density, and requiring the same density response, we find a Dyson-like equation relating the true and KS susceptibilities [93]. This is just the RPA equation well known in other areas, but with the Hartree interaction modified to include XC effects. One can further translate this problem into an eigenvalue problem [94], whose approximate solution for transition frequencies is [95]:

$$\omega \approx \omega_q + 2\langle q|\frac{1}{|\mathbf{r}-\mathbf{r}'|} + f_{\rm XC}|q\rangle \tag{22}$$

where

$$f_{\rm XC}[n_0](\mathbf{r}\mathbf{r}', t-t') = \delta v_{\rm XC}(\mathbf{r}t)/\delta n(\mathbf{r}'t')|_{n_0}. \tag{23}$$

is called the XC kernel. Thus, the effect of TDDFT is to produce corrections to the KS transitions to turn them into the true optical transitions of the system. If we had the *exact* $f_{\rm XC}(\mathbf{r}, \mathbf{r}', \omega)$ for the He atom density, calculated perhaps from a traditional wavefunction calculation, and inserted it in the full TDDFT response equations, we would get exactly the results of table 3.

4.2. TDDFT approximations

Most often, ground-state approximate XC functionals are used, even for the TD potential, which is called the adiabatic approximation. This often produces excellent excited-state properties, and transition frequencies typically within about 0.2 eV of the true numbers for molecules [98]. A simple example is the $\pi \rightarrow \pi^*$ transition in benzene in which, in a LDA calculation, the KS transition is at about 5 eV, but the TDDFT (ALDA) correction correctly shifts it to about 7 eV [99].

TDDFT has been implemented in many standard quantum chemistry codes, and is run routinely to extract electronic excitations of molecules [98]. However, as the number of calculations has grown very rapidly, the limitations of the scheme with an adiabatic XC approximation are being felt. Even early on [100], it was realized that Rydberg excitations would be missing within ALDA or AGGA, because of the poor quality potentials of the underlying ground-state approximation. The LDA potential of figure 7 is shallow and short ranged, and so has no Rydberg series. Exact exchange or SIC functionals take care of this [96]; figure 8 shows how accurate the LDA-SIC potential is in comparison. Also, double excitations can be shown to be missing within any adiabatic approximation [94], although frequency-dependent kernels can be constructed that restore them [101]. Charge transfer-type excitations also fail [102].

For solids, development has been slower, as the local and semi-local nature of approximate functionals means that their effect becomes negligible in the thermodynamic limit. This can be seen from the fact that the XC kernel in ALDA is independent of q, the wavevector in the Fourier transform of $\mathbf{r} - \mathbf{r}'$, as $q \rightarrow 0$, but the Hartree term grows as $1/q^2$. One cure for this problem is to use TD current DFT (TDCDFT) [103], whose validity is established in the first part of the RG theorem [91]. Related to this fact is the notion that no local approximation exists in terms of the density, but a gradient expansion in the current was constructed by Vignale and Kohn [104] for linear response. More recently, by comparison with solutions of the Bethe–Salpeter equation, accurate many-body approximations to the kernel have been constructed, yielding excellent results for excitonic peaks, etc [105].

The VK approximation is the only current-dependent approximation that is well established, and is often applied to problems where non-locality and memory (i.e. beyond adiabatic) effects are important. Most importantly, it often yields finite corrections where ALDA gives nothing, such as to the (0,0) component needed for the optical response of solids [103, 106], or the over-polarizability of long-chain conjugated polymers [73, 107]. But, given that it is a simple gradient expansion, its quantitative accuracy in any given situation is open to question [107–109].

4.3. Constitutive relations

We can relate the conductivity σ with the susceptibility χ described in section 4.1 using current continuity

$$\frac{{\rm d}n}{{\rm d}t} = -\nabla \cdot \mathbf{j}. \tag{24}$$

Since $\delta n(t) = \delta n {\rm e}^{{\rm i}\omega t}$, we have:

$$\delta n = -\frac{1}{{\rm i}\omega}\nabla \cdot \delta \mathbf{j}. \tag{25}$$

Then, using the relations between the vector potential and the field:

$$\delta \mathbf{E} = \frac{\partial \delta \mathbf{A}}{\partial t} = {\rm i}\omega \delta \mathbf{A}, \tag{26}$$

and the definitions of the current response:

$$\begin{aligned}\delta j_\alpha(\mathbf{r}\omega) &= \int {\rm d}^3\mathbf{r}' \sum_\beta \chi_{\alpha\beta}(\mathbf{r}\mathbf{r}'\omega)\delta A_\beta(\mathbf{r}'\omega) \\ &= \int {\rm d}^3\mathbf{r}' \sum_\beta \sigma_{\alpha\beta}(\mathbf{r}\mathbf{r}'\omega)\delta E_\beta(\mathbf{r}'\omega),\end{aligned} \tag{27}$$

where $\chi_{\alpha\beta}$ is the current–current response function, a tensor, and $\sigma_{\alpha\beta}$ is the conductivity tensor [110]. We get an

expression relating the response functions for conductivity and susceptibility:

$$\sigma_{\alpha\beta} = \frac{1}{\mathrm{i}\omega}\chi_{\alpha\beta}. \tag{28}$$

Also, going back to the definition of the density response and using the relations given above in equations (26) and (27), we obtain:

$$\delta n(\mathbf{r}\omega) = \frac{1}{\omega^2}\int \mathrm{d}^3 r \sum_\beta \partial_\alpha \sigma_{\alpha\beta}(\mathbf{r}\mathbf{r}'\omega)(-\partial'_\beta v(\mathbf{r}'\omega)) \tag{29}$$

which leads to the relation between the conductivity and susceptibility:

$$\sum_{\alpha\beta}\partial_\alpha\partial'_\beta\hat{\sigma}_{\alpha\beta}(\mathbf{r}\mathbf{r}'\omega) = -\mathrm{i}\omega\chi(\mathbf{r}\mathbf{r}'\omega). \tag{30}$$

As described in section 4.1, in TDDFT, there are three equivalent, exact formulae—usually studied in reference to the polarizabilities of atoms in strong fields—applied to different many-body descriptions and requiring different inputs, to describe the density response to an applied electric field.

There is an analogous response function for the current response to an external electric field. As with the density response formula, the response, given by the conductivity σ in this case, is different in each of the exact expressions. The many-body, non-local conductivity $\sigma(\mathbf{r}\mathbf{r}'\omega)$ describes the response to the external electric field $\delta\mathbf{E}_{\mathrm{ext}}$. The proper conductivity σ_{prop} is in response to the total field $\mathbf{E}_{\mathrm{tot}} = \mathbf{E}_{\mathrm{ext}} + \mathbf{E}_{\mathrm{H}}$, and the single-particle Kohn–Sham conductivity σ_S yields the response to the full expression for the electric field, $\mathbf{E}_{\mathrm{ext}}+\mathbf{E}_{\mathrm{H}}+\mathbf{E}_{\mathrm{XC}}$, including the unphysical XC contributions $\mathbf{E}_{\mathrm{XC}}$.

$$\begin{aligned}\delta\mathbf{j}(\mathbf{r}\omega) &= \int \mathrm{d}r\, \sigma(\mathbf{r},\mathbf{r}',\omega)\,\delta\mathbf{E}_{\mathrm{ext}}(\mathbf{r},\omega) && \text{(MB)}\\ &= \int \mathrm{d}r\, \sigma_{\mathrm{prop}}(\mathbf{r},\mathbf{r}',\omega)\,\delta\mathbf{E}_{\mathrm{tot}}(\mathbf{r},\omega) && \text{(EM)}\\ &= \int \mathrm{d}r\, \sigma_{\mathrm{s}}(\mathbf{r},\mathbf{r}',\omega)\,\delta\mathbf{E}_{\mathrm{s}}(\mathbf{r},\omega). && \text{(DFT).}\end{aligned} \tag{31}$$

4.4. DC transport from Kubo response

In the limiting case of weak bias, the response can be expanded to first order in the electric field. In this, we follow the logic of Kamenev and Kohn [111]. To derive the DC transport response, a frequency-dependent electric field is applied, and the limit $\omega \to 0$ is taken while always ensuring that $v_{\mathrm{F}}/\omega \ll L$, where L is the circumference of the ring. As shown by Kamenev and Kohn, this reproduces the Landauer formula for weak bias for Hartree-interacting electrons. Our work can be regarded as a simple extension of this analysis to DFT. Note that extreme care must be taken in the limiting procedure to extract the relevant results [112–114].

It can be shown that, as $\omega \to 0$, the conductivity can be rewritten as the transmission coefficient familiar from the Landauer formulation. This limit has to be performed carefully to obtain the correct current. It has to be assured that the excursion length of electrons in the device, given by $l_{\mathrm{F}} = \frac{v_{\mathrm{F}}}{\omega}$, is smaller than the region of the density response, l_ρ, which in turn has to be smaller than the device dimensions L of the extended molecule in the DFT calculation (see figure 3).

Using the (DFT) response equation for the Kohn–Sham susceptibility and the full expression for the field we can obtain the correct current. We first rewrite the Kohn–Sham non-local conductance as

$$\hat{\sigma}_{\mathrm{s}}(\mathbf{r}\mathbf{r}'\omega) = \Big(n_0(\mathbf{r})\,\delta^{(3)}(\mathbf{r}-\mathbf{r}')\,\mathbb{I} + \hat{R}(\mathbf{r}\mathbf{r}'\omega)\Big)\Big/(\mathrm{i}\omega) \tag{32}$$

where

$$\hat{R}(\mathbf{r}\mathbf{r}'\omega) = \frac{1}{2}\sum_q \frac{\mathbf{P}_q(\mathbf{r})\mathbf{P}_q^*(\mathbf{r}')}{\omega+\omega_a+\mathrm{i}0_+}, \tag{33}$$

defining $\mathbf{P}_q(\mathbf{r}) = \phi_i^*(\mathbf{r})\nabla\phi_j(\mathbf{r}) - \phi_j(\mathbf{r})\nabla\phi_i^*(\mathbf{r})$. Here $\phi_i(\mathbf{r})$ and ϵ_i are the KS orbitals and eigenvalues, $\omega_a = \epsilon_i - \epsilon_j$, and $q = (i, j)$. This result can be written more compactly in terms of the retarded KS Green's function $G_{\mathrm{s}}^r(\mathbf{r}\mathbf{r}'\epsilon)$ and the corresponding KS spectral density

$$A_{\mathrm{s}}(\mathbf{r}\mathbf{r}'\epsilon) = -\operatorname{Im} G_{\mathrm{s}}^r(\mathbf{r}\mathbf{r}'\epsilon)/\pi, \tag{34}$$

just as the regular χ_{s} can be. Thus we find, exactly,

$$\begin{aligned}\hat{R}(\mathbf{r}\mathbf{r}'\omega) = \tfrac{1}{2}\int \mathrm{d}\epsilon f(\epsilon)\{&G_{\mathrm{s}}^r(\mathbf{r}\mathbf{r}',\epsilon+\omega)\\ &+ (G_{\mathrm{s}}^r)^*(\mathbf{r}\mathbf{r}',\epsilon-\omega)\}\overleftrightarrow{\nabla}\overleftrightarrow{\nabla}'A_{\mathrm{s}}(\mathbf{r}\mathbf{r}'\epsilon).\end{aligned} \tag{35}$$

For small ω, only the imaginary component of the KS Green's function contributes to $\hat{R}$. Expansion in powers of ω yields a term linear in ω, and an integration by parts yields the DC conductance entirely in terms of the spectral density at the Fermi energy [111]:

$$\hat{\sigma}_{\mathrm{s}}(\omega\to 0) = -\pi A_{\mathrm{s}}(\epsilon_{\mathrm{F}},\mathbf{r},\mathbf{r}')\overleftrightarrow{\nabla}\otimes\overleftrightarrow{\nabla}'A_{\mathrm{s}}(\epsilon_{\mathrm{F}},\mathbf{r},\mathbf{r}'). \tag{36}$$

This result is true for the conductance of non-interacting electrons in any single-particle potential. Next, we specialize to a 1D system, to avoid complications. Then, equation (30) tells us that, as $\omega \to 0$, σ_{s} becomes independent of position. Thus, σ_{s} from equation (36) may be evaluated at any choice of z and z'. An easy choice is $z < 0$ and $z' > 0$, and one finds [111]

$$\sigma_{\mathrm{s}}(\omega\to 0) = \frac{T_{\mathrm{s}}(\epsilon_{\mathrm{F}})}{\pi}. \tag{37}$$

Since $\sigma_{\mathrm{s}}(\omega\to 0)$ is just a constant, it can be taken outside the integral of equation (32), yielding

$$\delta I = \frac{T_{\mathrm{s}}}{\pi}(\delta V_{\mathrm{tot}} + \delta V_{\mathrm{XC}}) \tag{38}$$

$$\delta I(\omega\to 0) = \frac{T_{\mathrm{s}}(\epsilon_{\mathrm{F}})}{\pi}\int \mathrm{d}^3 r'(\delta E_{\mathrm{ext}}(\omega) \tag{39}$$

$$+\delta E_{\mathrm{H}}(r'\omega) + \delta E_{\mathrm{XC}}(r'\omega)) \tag{40}$$

where $\delta V_{\mathrm{tot}} = \int \mathrm{d}z'\,\delta E_{\mathrm{ext}}(\omega) + \delta E_{\mathrm{H}}(z'\omega)$ is the net drop in total electrostatic potential across the device, and

$$\delta V_{\mathrm{XC}} = \int_{-\infty}^{\infty}\mathrm{d}z\,\delta E_{z,\mathrm{XC}}(z,\omega\to 0) \tag{41}$$

is the corresponding drop (if any) in the XC potential.

Thus, equation (42) would be exact if the exact V_{XC} was properly included. But the implementation commonly

used in the Landauer formulation of molecular electronics corresponds, as we will see below in 4.5, to only the Hartree response:

$$\delta I = \frac{1}{\pi}\int_{\mu}^{\mu+\delta V} \mathrm{d}\epsilon\, T_{\mathrm{s}}(\epsilon, V)(f_{\mathrm{L}}(\epsilon) - f_{\mathrm{R}}(\epsilon)) = \frac{T_{\mathrm{s}}(\epsilon_{\mathrm{F}})}{\pi}\delta V_{\mathrm{tot}} \qquad \text{(LANDAUER)}. \tag{42}$$

Equations (38) and (42) are identical, except that the standard approach does not include the extra exchange–correlation term, δV_{xc}. This derivation has been recently generalized to include correct averaging over the lateral directions [115].

4.5. XC correction to current

The present implementation of the Landauer formulation using local functionals includes the Hartree piece of the potential and thus correctly includes the charging effects, but it is missing the XC piece. To see this, consider the XC contribution to the voltage given by equation (41). Since $\delta E_{\mathrm{xc}} = -\nabla \cdot \delta v_{\mathrm{xc}}$, this implies that $\delta V_{\mathrm{xc}} = \delta v_{\mathrm{xc}}(z \to \infty) - \delta v_{\mathrm{xc}}(z \to -\infty)$. But far from the barrier, $\delta\rho = 0$, and so any local or semi-local approximation necessitates that δv_{xc} equals zero far from the barrier. Thus $\delta V_{\mathrm{xc}} = 0$ when working within these approximations [19]. Thus ALDA and all other local or semi-local approximations miss the non-local interactions of the exact XC functional.

Alternatively, integration of the second equation in expressions (32) would also give the exact result since all three formulae are equivalent and exact:

$$\delta I = \frac{T_{\mathrm{prop}}}{\pi}\delta V_{\mathrm{tot}} \tag{43}$$

but T_{prop} refers to the full proper transmission coefficient which cannot be easily calculated for a realistic system, and is not the transmission through any single-particle potential.

TDDFT within a local or semi-local approximation has been shown to produce erroneous results when non-local effects become important, such as in the optical response of solids. The Vignale–Kohn functional is a non-local functional in terms of current density that has been successfully applied to situations where non-locality cannot be ignored, such as in long conjugated polymers [73, 107, 116] where local approximations give overestimates on the static polarizabilities. This non-locality also plays a role in the non-equilibrium transport problem as seen in section 4.4. In the regime of weak bias, Koentopp *et al* [19] estimate the size of the XC correction to the current in the Vignale–Kohn approximation. Since ALDA is a local approximation, it misses the non-local interactions of the exact XC functional. Inclusion of the viscous contribution to δV_{xc} yields a correction to the transmission coefficient that reduces its magnitude:

$$\delta V_{\mathrm{xc}}/V \approx -(1 - T(\epsilon_{\mathrm{F}}))T(\epsilon_{\mathrm{F}})/40\pi^{1/2}k_{\mathrm{F}}^{3/2}. \tag{44}$$

A more explicit expression for the XC correction can be calculated. Sai *et al* [20] calculate the dynamical response contribution to current flow using the Vignale–Kohn correction in TDCDFT. This dynamical contribution is a viscous flow component from the XC field that is missing in ground-state DFT calculations and gives a finite correction to the conductance. A current density functional theory is necessary because functionals that are dependent on the density alone do not contain information about the constant value of the current. The Vignale–Kohn construction has an XC field that has both the ALDA XC potential and a term dependent on the XC stress tensor which in turn is dependent on viscoelastic coefficients and velocity fields.

A dynamical resistance R^{dyn} arises from the DC XC field which increases the total resistance of the system, thus acting against the external field.

$$R^{\mathrm{dyn}} = \frac{4}{3\mathrm{e}^2 A_{\mathrm{c}}}\int_{-\infty}^{\infty}\eta\frac{(\partial_z n)^2}{n^4}\,\mathrm{d}z \tag{45}$$

where a and b are points inside the electrodes, A_{c} is the cross-sectional area, n is the density, and η is the viscosity. A calculation that includes the real part of the stress component of the electric field yields a correction of 10% [20].

5. Finite bias

Given the limitations of the *standard approach* already discussed, it has been realized that a more fundamental derivation of the conductance formula is needed, especially one that lends itself to a DFT treatment. For example, in DFT, one is not allowed to turn off the coupling between the molecule and leads, as the Hohenberg–Kohn theorem does not apply in empty space, nor does the RG theorem allow for time-dependent interactions between electrons.

Several suggestions have been made as to how to do this, that might appear quite different. Here we discuss and compare just two of these: the master equation approach, and the TDDFT–NEGF approach. The master equation requires coupling to a dissipative bath, such as the phonons, in order to achieve a steady current, while the TDDFT–NEGF approach achieves a steady current via dephasing into the continuum. Moreover, the master equation allows for periodic boundary conditions (PBCs) whereas TDDFT–NEGF uses a localized system. Finally, because of this, the master equation with periodic boundary conditions requires TD current DFT, whereas TDDFT–NEGF uses the density as the basic variable.

5.1. Master equation

5.1.1. Periodic boundary conditions. The Landauer formulation, and indeed most of the literature on transport, uses the concept of different chemical potentials on the left- and right-electrodes, and assumes some steady current-carrying state between them.

Such a situation is not so easy to realize within the basic theorems of density functional theory, time-dependent or otherwise. Even TDDFT requires starting from some initial wavefunction [117], almost always the ground-state wavefunction of some system. But the ground state of any system of electrons has at most one chemical potential, not two.

Thus useful DFT descriptions begin with a system in its electronic ground state, and a single chemical potential.

So far, only the situation in which both electrodes are of the same metal have been investigated. Furthermore, to avoid the difficulties of having infinite potentials far inside the electrodes, a gauge transformation that is standard in solid-state physics is applied and a solenoidal magnetic field is imposed on a ring of material. A vector potential that is linear in time, $a = Et$ then gives rise to a uniform electric field on the ring, causing a current to flow.

The same approach is then applied to finite bias, and again avoids the need for two different chemical potentials. However, a new complication arises, as in the presence of the electric field, as $\omega \to 0$, if L is kept finite, the electrons will accelerate indefinitely around the ring, which is not the situation we wish to model. Instead, if some coupling to the phonons in the system is introduced, there will be dissipation, and a steady state can develop. It is possible to derive an extension of TDCDFT that includes dissipation in a time-dependent Kohn–Sham master equation. Note that dissipation is unnecessary in the weak bias limit of the previous section, as Joule heating is second order in the perturbation [118].

5.1.2. Master equation theory. A master equation approach has been constructed that introduces dissipation via a quantum mechanical treatment of the Boltzmann equation from statistical mechanics [74]. The master equation describes the evolution of the density of a system coupled to a heat bath and has an analogue with the well studied problems of optical interactions of laser fields with matter [119]—atomic transitions in the presence of electromagnetic fields. Among the advantages of this approach is the elimination of the artificial boundary and contact conditions necessary in the Landauer formulation, the inclusion of inelastic processes, and applications beyond the steady state situation.

With this approach, there are no reservoirs corresponding to the left and right leads at different chemical potentials and the voltage drop across the barrier is an output of the method rather than an input as it is for the Landauer approach. Instead of the open boundary conditions employed by the Landauer approach as illustrated in figure 3, periodic boundary conditions are imposed [74] such that the system is a closed circuit with no exchange of electrons with semi-infinite reservoirs (see figure 12). This geometry is a neat way to treat an open system, avoiding partitioning an infinite system as in the *standard approach*.

The approach employs a quantum Liouville equation for the total Hamiltonian of the system H_{T}, which contains the device Hamiltonian H_0, the phonon bath R, and the electron–phonon coupling potential V. S_{T} is the density matrix for the total system. Its time evolution is given by

$$\mathrm{d}S_{\mathrm{T}}/\mathrm{d}t = -\mathrm{i}[H_{\mathrm{T}}, S_{\mathrm{T}}]. \tag{46}$$

After tracing out the bath degrees of freedom, what results is the Liouville equation for the reduced density matrix S along with a term that encapsulates the dissipation in the system $C[S]$:

$$\mathrm{d}S/\mathrm{d}t = -\mathrm{i}[H, S] + C[S]. \tag{47}$$

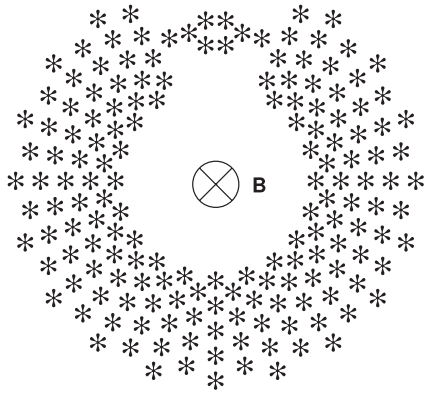

Figure 12. Master equation schematic diagram—periodic boundary conditions, magnetic field induces electric field on ring.

The dissipation term describes collisions with the heat bath and is given by

$$C[S] = -\sum_{m,n} \Gamma_{mn}(L_{nm}L_{mn}S + SL_{nm}L_{mn} - 2L_{mn}SL_{nm}), \tag{48}$$

where $L = c_n^\dagger c_m$ and Γ_{mn} are the transition probabilities obtained through Fermi's golden rule. To derive explicit expression, the coupling potential

$$V = \sum_{m,n,\alpha} \gamma_{m,n}^{\alpha} c_n^\dagger c_m a_\alpha^\dagger + \mathrm{h.c.} \tag{49}$$

is treated perturbatively to second order. The creation and destruction operators for the electrons/phonons are $c^\dagger/c$ and $a^\dagger/a$ respectively. In the coupling matrix elements, $\gamma_{m,n}^{\alpha}$, the indices m and n refer to the electrons and α refers to the phonons. Γ_{mn} is then given by:

$$\begin{aligned} D(\epsilon_n - \epsilon_m)|\gamma_{mn}|^2(\bar{n}_{\epsilon_n-\epsilon_m} + 1), &\qquad \epsilon_n > \epsilon_m \\ D(\epsilon_m - \epsilon_n)|\gamma_{mn}|^2\bar{n}_{\epsilon_m-\epsilon_n}, &\qquad \epsilon_m > \epsilon_n. \end{aligned} \tag{50}$$

The electric field is imposed on the system through the addition of a time-dependent vector potential $a(t)$ in the Hamiltonian. Gauge transformations are then performed periodically to set the vector potential to zero, otherwise the Hamiltonian would grow indefinitely leading to numerical instability in the implementation. One of the problems with previous attempts to use a master equation formulation within this set-up is the apparent current continuity violation. But it can be shown that current continuity is maintained once the dissipative contribution to the current is considered [74]. The equation of motion for the time-dependent density when propagating the system under the master equation is given by

$$\left.\frac{\mathrm{d}\langle n(r)\rangle}{\mathrm{d}t}\right|_{t=0} = -\nabla\langle j(r)\rangle + \mathrm{Tr}(n(r)C[S]\bar{S}). \tag{51}$$

The last term in this equation is the contribution due to the dissipative part of the master equation and so the total current is then given by the standard expression using the current operator plus a dissipative part due to the propagation of the system under the master equation:

$$\langle j_{\mathrm{T}}(r)\rangle = \langle j(r)\rangle + \langle j_{\mathrm{D}}(r)\rangle. \tag{52}$$

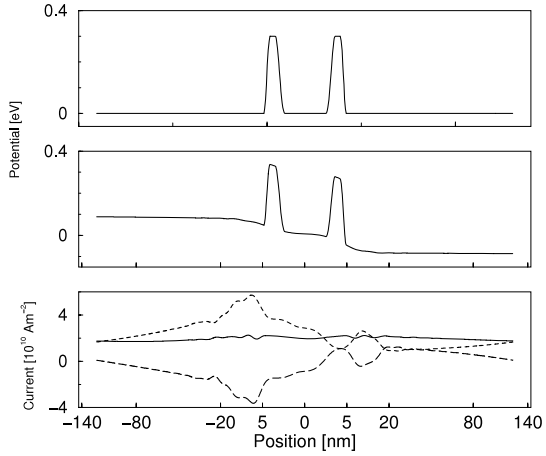

Figure 13. Potential for the DBRTS. Top panel—no applied external field, middle panel—external field for the case of low dissipative coupling, γ_0. The bottom panel shows the total current (solid line), the Hamiltonian current (short dashed line) and the dissipative current (dashed line).

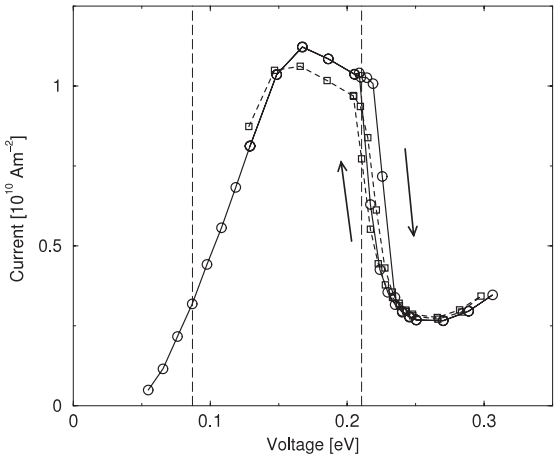

Figure 14. Hysteresis effects for a DBRTS device as demonstrated through I–V plots for two different values of dissipative coupling γ_0. Lower γ_0 is associated with a more pronounced hysteresis.

The general many particle formulation must be simplified to an effective single particle form to be of any use in practice. The many-body density matrix S that satisfies the Liouville equation for a Hamiltonian H, must be rewritten in an effective single-particle description such that the resulting single-particle density matrix S_s is in terms of the eigenstates of H_s. These eigenstates are the equilibrium single-particle eigenstates and are related to S_s via the expression $S_s = \sum_{lm} f_{lm}|l\rangle\langle m|$. The density functional formulation which maps a system of interacting particles into one of non-interacting particles with the same density is a natural direction to proceed. In analogy with the Hohenberg–Kohn theorem for ground-state DFT and the Runge–Gross theorem for TDDFT, it can be proven that for a fixed electron–electron interaction, a given $C[S]$ and an initial density matrix S_0, the potential is uniquely determined by its time-dependent density $n(\mathbf{r}t)$. A single-particle form of equation (47) can be recovered by applying perturbation theory for a weak interaction between the non-interacting electrons and the phonons in the bath, tracing out the irrelevant degrees of freedom, and adding the Hartree potential to the single-particle Hamiltonian. What results is a single-particle form of the master equation with a Kohn–Sham version of $C[S]$ and a single-particle form of the density matrix expressed in the basis of the equilibrium single-particle eigenstates indexed by n, m. If the expansion coefficients are related to the many-body density matrix S via $f_{nm} = \mathrm{tr}[Sc_m^\dagger c_n]$, then the single-particle master equation can be written in terms of the single-particle eigenstates:

$$\frac{\mathrm{d}f_{nm}}{\mathrm{d}t} = -\mathrm{i}\sum_p [H_{np}(t)f_{pm} - f_{np}H_{pm}(t)] + (\delta_{nm} - f_{nm})\sum_p(\Gamma_{np} + \Gamma_{mp})f_{pp} - f_{nm}\sum_p(\Gamma_{pn} + \Gamma_{pm})(1 - f_{pp}). \quad (53)$$

In addition, the parameters in the dissipative part of the Kohn–Sham master equation (see equation (50)) can be in principal obtained from ground-state DFT linear response calculations, thereby eliminating the need for any empirical parameters.

5.1.3. Master equation results. The master equation approach is currently under development, but some initial results for test systems have been calculated [120, 121]. The first model tested with the master equation approach was a simple 1D double barrier resonant tunnelling system (DBRTS). Well known results familiar to the experimental community were derived for a DBRTS and show that the effect of inelastic collisions, accounted for in the master equation formulation, is important in understanding the behaviour of these devices.

Among the approximations made for the phonons in this model calculation are, that their density of states has a parabolic dependence given by $D(\omega) \approx \omega^2$. Furthermore, the coupling between levels m and n is set to a constant $\gamma_{mn} = \gamma_0$. In the top two panels of figure 13, results for the potential in the absence of a field and in the presence of a field with low dissipative coupling γ_0 are given. Results are similar to the results from the Landauer formulation except for the following important points.

The voltage drop across the device is an output of the calculation rather than an input and there can be seen a small voltage drop across the wire as well, but this is soon neutralized by screening effects.

The bottom panel of figure 13 displays the total current derived. In keeping with the constraints of current continuity, the total current (solid line) is constant within numerical error due to cancellation between the Hamiltonian current (short dashed line) and the dissipative current (long dashed line). It should also be noted that the dissipative current is larger at the contact points, indicating that these are the sites of local Joule heating.

The master equation approach also predicts the hysteresis effects of a DBRTS as demonstrated in figure 14. At low dissipative coupling γ_0, the hysteresis is much more evident than at higher values of γ_0. For stronger dissipative coupling, the resonance peak also shifts towards lower voltages.

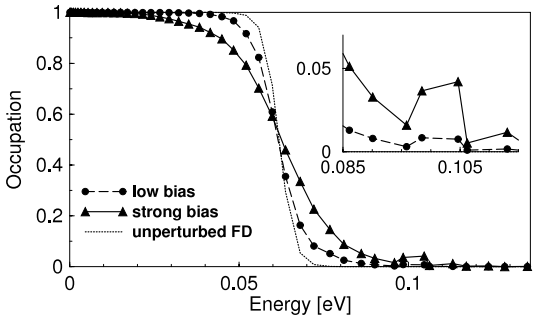

Figure 15. Electron occupation of the resonant level in a DBRTS as given by the diagonal elements of the density matrix in the steady state. A higher bias leads to non-linear effects as evidenced by stronger deviations from the unperturbed Fermi–Dirac distribution.

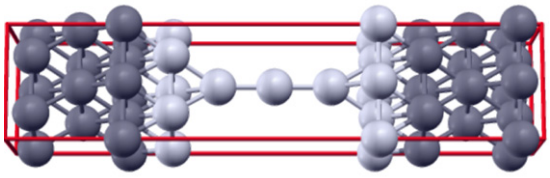

Figure 16. Three atom gold chain: supercell geometry showing the atomic wire connected to two gold electrodes (Au 111 surfaces). The dark atoms indicate the region where dissipative coupling is present. Periodic boundary conditions are applied in all directions. The lateral interaction between a wire and the nearest periodic images has negligible effect on the current.

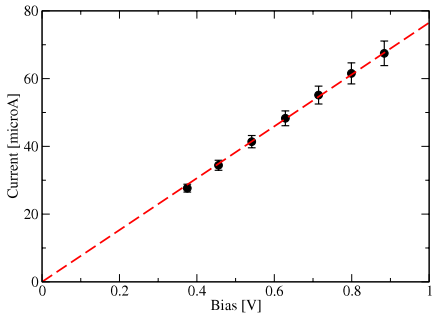

Figure 17. Calculated I–V characteristics of a 3 atom gold wire. The black dots are the master equation results. The dashed line indicates the characteristics corresponding to one quantum of conductance. The error bars reflect the fluctuations of the Hamiltonian current in the supercell which measure deviation from current continuity in the numerical calculation.

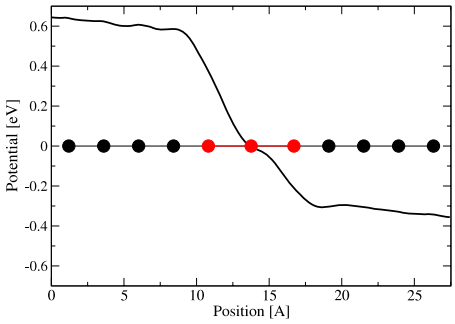

Figure 18. 3 atom gold chain—potential: total potential (including external potential, and induced Hartree and exchange–correlation potential) averaged over planes perpendicular to the wire. The external potential in the supercell is given, for illustrative purposes, in the position gauge (which does not satisfy the periodic boundary conditions). The black dots indicate the position of the atomic planes in the slab, whereas the red dots indicate the atoms of the wire. The total potential is essentially flat in the electrodes. The large drop across the wire is due to the contact resistance.

In figure 15, the electron occupation of the level is plotted for different values of the applied bias. At higher bias, the distribution deviates from equilibrium and exhibits a bump in the tail that points to charging of the resonant level. This charging is the origin of the bistability and the hysteresis observed in DBRTs. The bistability arises from the non-linearity associated with the Hartree potential. The finite current for voltages above the resonance peak stems from the inclusion of dissipation. In the absence of dissipative effects the current would go down to zero the moment the resonant level becomes fully occupied and the broadened level no longer overlaps with the Fermi level of the lead. When dissipation is included, electrons can relax into the leads leading to a finite current for bias voltages above the resonance. The dissipative coupling also controls the size of the hysteresis effect.

5.1.4. Chains of gold atoms. Further calculations within the master equation approach have studied electronic transport through a 3 atom gold wire sandwiched between two Au(111) surfaces [121]. Figure 16 shows the unit cell of the periodic system used in the calculations. Four layers of gold atoms per side are included as the contacts. Dissipation is applied in the three outermost atomic layers only. Again, the phonon density is assumed to be parabolic and the coupling takes the form of $\gamma_{ij} = \gamma \langle i|V|j\rangle$ where γ sets the strength of the dissipation.

In this application, where a very small periodically separated cell was used, a very large dissipative coupling was necessary to force a steady state (this was obtained by imposing one quantum of conductance at once specific value of the applied bias). This leads to an unphysically large dissipative current. The strength of the dissipative coupling can be reduced with increasing system size, eventually reaching its physical value for cells that are large compared to the electron–phonon mean free path. Under those conditions the Hamiltonian current dominates. It was found that a more physical behaviour of the I–V characteristics is obtained, when only the Hamiltonian current is used to model the physical current. Neglect of the dissipative current in this system is further supported by the fact that the current continuity violation of the Hamiltonian current is weak (see figure 17).

The calculated I–V-characteristics, shown in figure 17 reproduces well the linear behaviour measured experimentally [2, 3, 5]. In figure 18 we plot the total (external plus induced) potential across the device. The potential drops occurs mainly across the length of the Au wire. Only a small portion of the potential drop occurs inside the leads. We would expect no potential drop at all inside a perfect metal, the small observed drop is due to the dissipation in the three outermost atomic layers of the leads.

5.2. TDDFT–NEGF

Another method that avoids the use of two external chemical potentials with an artificial partitioning and manages to obtain a steady current in transport calculations is the exact non-equilibrium Green's function approach using time-dependent density functional theory (TDDFT) [75–77, 122, 123]. The system begins in thermodynamic equilibrium in its ground state and the leads and device are coupled. A time-dependent perturbation is imposed deep inside the leads, such that the potential exhibits a step somewhere inside the molecule.

The method applies the NEGF Keldysh formulation to the time-dependent KS equations, i.e., to a set of non-interacting particles yielding the correct density. The time evolution of the system is then described by the KS equations of TDDFT

$$\mathrm{i}\dot{\Psi}_\mathrm{s}(\mathbf{r},t) = H_\mathrm{s}(\mathbf{r},t)\Psi_\mathrm{s}(\mathbf{r},t), \tag{54}$$

where $H_\mathrm{s}(\mathbf{r},t)$ is the time-dependent KS Hamiltonian, and $\Psi_\mathrm{s}(\mathbf{r},t)$ is the KS wavefunction. Using the continuity equation $\partial/\partial t\, n(\mathbf{r},t) = -\nabla \mathbf{j}_\mathrm{s}(\mathbf{r},t)$ for the KS current density $\mathbf{j}_\mathrm{s}(\mathbf{r},t)$ this produces the correct time-dependent current through the device:

$$I(t) = -\int \mathrm{d}^3 r \frac{\mathrm{d}}{\mathrm{d}t} n(\mathbf{r},t) \tag{55}$$

where the integral is over some cross-section through the molecule. In NEGF, the density can be expressed in terms of the lesser Green's function:

$$n(r,t) = -2\mathrm{i}G^<(r,t;r,t) \tag{56}$$

which in turn can be calculated from equations of motion for the non-interacting system. To solve the non-interacting problem, the system is partitioned into the molecule (C), and left/right leads (L, R) as in the *standard approach* (see section 2.3). The KS Hamiltonian can then be written as a 3×3 block matrix, yielding for the time evolution

$$\mathrm{i}\frac{\partial}{\partial t}\begin{bmatrix}\Psi_\mathrm{L}\\ \Psi_\mathrm{C}\\ \Psi_\mathrm{R}\end{bmatrix} = \begin{bmatrix}H_\mathrm{LL} & H_\mathrm{LC} & 0\\ H_\mathrm{CL} & H_\mathrm{CC} & H_\mathrm{CR}\\ 0 & H_\mathrm{RC} & H_\mathrm{RR}\end{bmatrix}\begin{bmatrix}\Psi_\mathrm{L}\\ \Psi_\mathrm{C}\\ \Psi_\mathrm{R}\end{bmatrix}, \tag{57}$$

where $\Psi_\alpha(\mathbf{r},t)$ is the KS wavefunction projected onto left/right lead (L, R) and the molecule region (C), respectively.

For the left and right lead ($\alpha = \mathrm{L}, \mathrm{R}$), we can, using the lead Green's functions $\mathbf{g}_\alpha$ (see description in section 2.3), obtain an explicit solution for the projected wavefunctions:

$$\Psi_\alpha(t) = \mathrm{i}\mathbf{g}_\alpha(t,0)\Psi_\alpha(0) + \int_0^t \mathrm{d}t' \mathbf{g}_\alpha(t,t')H_{\alpha C}\Psi_\mathrm{C}(t'). \tag{58}$$

$\mathbf{g}_\alpha$ is defined via $(\mathrm{id}/\mathrm{d}t - H_{\alpha\alpha}(t))\mathbf{g}_\alpha(t,t') = \delta(t-t')$ with the appropriate boundary conditions $\mathbf{g}_\alpha(t^\dagger,t) = -\mathrm{i}$ and $\mathbf{g}_\alpha(t,t^\dagger) = 0$.

Using this, we can rewrite the expression for the molecule region as

$$\mathrm{i}\frac{\partial}{\partial t}\Psi_\mathrm{C}(t) = H_\mathrm{CC}(t)\Psi_\mathrm{C}(t) + \int_0^t \mathrm{d}t' \Sigma(t,t')\Psi_\mathrm{C}(t') + \mathrm{i}\sum_{\alpha=\mathrm{L},\mathrm{R}} H_{\mathrm{C}\alpha}\mathbf{g}_\alpha(t,0)\Psi_\alpha(0). \tag{59}$$

where

$$\Sigma(t,t') = H_\mathrm{CL}(t)\, g_\mathrm{L}(t,t')\, H_\mathrm{LC}(t') + H_\mathrm{CR}(t)\, g_\mathrm{R}(t,t')\, H_\mathrm{RC}(t') \tag{60}$$

is the self-energy accounting for coupling to the leads as described in section 2.3. Thus equation (59) yields, in principle exactly, the time evolution of the molecular wavefunction in the presence of a current through the leads. It is non-Hermitian, as it describes electrons flowing from left to right. The solution for the wavefunction of the central region is obtained by propagating an initial state, i.e. the ground state of the extended system in equilibrium, which is obtained in a fashion analogous to the *standard approach*. For the actual propagation, transparent boundary conditions are imposed at the lead interfaces and a generalized Cayley method is used (see [123] for details).

The feasibility of the scheme has been tested on simple 1D systems. These calculations demonstrate the independence of the steady current on the history, and show a variety of features, such as non-monotonic dependence of current on bias, and larger transient currents than steady state currents. First applications of this approach include: (i) the study of the role of bound states in transport [124]. Here oscillations in the density and the TDDFT KS potential have been observed, the system does not evolve towards a steady state. (ii) The coupling to nuclei [125]. However, these are all non-interacting problems, and so have not tested the procedure when interaction plays a roll.

An important issue of the formalism is whether or not a steady current can arise in the absence of any dissipation. For non-interacting electrons (e.g. the electrons in the KS system), it has been found a steady current develops if

(1) the single-particle Hamiltonian becomes time-independent as $t \to \infty$,
(2) the electrodes form a continuum of states, i.e., are infinite,
(3) local density of states on the molecule is smooth.

These all appear reasonable conditions. Furthermore, the steady current is independent of the history of the turning on of the potential step, if the $t \to \infty$ Hamiltonian is.

The crucial point for the steady current is the second one. In the presence of a continuum of states, even non-interacting electrons dephase and a steady current develops. This is the mechanism for achieving a steady current in this approach, and makes dissipation to phonons or many-body scattering effects unnecessary. A continuum of states requires infinite electrodes, but these are then implicitly included in source and sink terms in the resulting equations.

5.3. Master equation versus TDDFT–NEGF

Both the master equation approach and the TDDFT–NEGF approach go beyond the *standard approach*. Each begins from a situation for which we have a basic theorem proving a functional dependence of the potential on the density, and from which the Landauer formula can be derived, at least in the case of non-interacting electrons. They clearly yield different results in cases where their conditions differ, such as when

dissipation is strong in the master equation, but it is as yet unknown if they differ when applied to the same situation (and if they do, which one is 'correct'). In this section, we compare and contrast the two different approaches.

Basic variable: In the master equation approach, because the system experiences a solenoidal magnetic field and periodic boundary conditions are used, the basic variable is the current density. In contrast, the TDDFT–NEGF approach has been developed using the density itself as the basic variable. While this is more familiar within DFT, the current allows development of simple approximations such as Vignale–Kohn, yielding simple corrections to the conductance.

Boundary conditions: Almost all present calculations are performed on localized systems embedded between two electrodes, using localized basis sets, and this is also true for TDDFT–NEGF. The master equation approach both requires and allows use of plane-wave codes, and so can make it much easier to adapt present solid-state codes for use in transport calculations.

Fundamental theorems: TDDFT–NEGF is based on the Runge–Gross theorem, which applies only to finite systems. Yet the leads must be infinite to produce the required dephasing. This is an inconsistency in the approach whose implication is debatable. The master equation, on the other hand, required proving the Runge–Gross theorem for the master equation instead of the time-dependent Schrödinger equation, and so requires introducing new functionals. These may (or may not) reduce to the standard ones of TDCDFT in the limit of weak dissipation.

Need for dissipation: The TDDFT–NEGF approach demonstrates that a steady current can arise *without* explicit dissipation mechanisms, once the leads are infinite. The master equation approach may well reduce to the same result in the limit in which the ring size is very large and the dissipation small, but this has yet to be demonstrated. If so, they become, in that limit, simply two different procedures for finding the same result. If not, one might well be correct for molecular conductance, the other not.

Weak bias: With small dissipation, the master equation produces the same conductance in the zero bias limit as the Kubo response [74], and therefore includes the XC corrections to the Landauer formula as seen in section 4.4. A similar result can be derived from the TDDFT–NEGF formula [122], although couched in DFT terms. Thus the formalisms agree in the limit of weak bias and small dissipation, even for interacting electrons. For the description of Joule heating effects and phonon scattering, which are not easily incorporated into the TDDFT–NEGF approach, the master equation formalism provides a natural framework.

6. Summary

In this brief, non-comprehensive review, we have critically examined the present state of the art of DFT calculations of transport through single molecules. Our findings are:

- Even the steady state of current flowing through a molecule is not included by the basic theorems establishing ground-state DFT.
- The commonly used approximation of *ground-state* DFT in the Landauer formula, which we dub the *standard approach*, has a variety of limitations, making it inexact, even if the exact ground-state functional were known and used.
- Standard density functional approximations, such as LDA, GGA, or hybrids, are insufficiently accurate to treat molecules weakly coupled to leads, and likely produce large overestimates of the current. This effect might be the origin of the overestimates relative to experiment. Orbital-dependent functionals, such as exact exchange or self-interaction corrected LDA (LDA-SIC), should perform much better.
- The *standard approach* is only a Hartree-level theory for the conductance, and neglects non-local XC corrections to the conductance. This is demonstrable in the case of weak bias. Either orbital-dependent or current-dependent functionals are needed to even estimate these corrections.
- For finite bias, several approaches have been developed that are within time-dependent DFT frameworks, thus addressing the problem of the inadequate ground-state approximation. Two of these have been described in this review. (i) The master equation approach which includes dissipation to phonons. (ii) The TDDFT–NEGF formalism which does not have the need for dissipation. Connections are being developed between the two, and time will tell which is more practical, reliable, or relevant.

Open questions for both new approaches and any other DFT treatments include the following:

- Do they agree with the Kubo response weak bias limit discussed in section 4.4? Both new formalisms do this.
- At finite bias, which effects are included or not in each approach?
- At finite bias, in what limits do they agree or disagree with each other and with the standard approach? We already know that within ALDA, all give the same answer as the standard approach, but expect differences with non-local non-adiabatic functionals.
- Does one always approach a steady state, and is it unique? The hysteresis seen in model calculations with the master equation is an example of more than one steady solution.
- Is there a dependence on how the potential is turned on? Recently, bound states of the molecule have been shown to lead to infinitely oscillating contributions to the current in model calculations using the TDDFT–NEGF approach, when the turn-on is non-adiabatic. Do these survive in an interacting system?
- Are there infinite memory effects in the time-dependent Kohn–Sham potential? These are logically possible, and might even be necessary, to reproduce the physics.
- Exactly what features of these theories are needed to reproduce strongly correlated effects such as Coulomb blockade, and is there any chance to model such features?

On the other hand, the present Landauer-type calculations (the standard approach) yield the correct steady solution to the more sophisticated approaches *when the functional is local in time and space* (see section 4.4), and this may be sufficient for

many purposes. Only more demanding calculations (be they time-dependent DFT, non-local static DFT, or CI or GW) and better characterized experiments can tell us what is important to reliable first-principles predictions of the conductance of single molecules.

Acknowledgments

The authors are very grateful to H Baranger, F Evers, R Gebauer, N Lang, S Piccinin, E Prodan, S Sanvito and W Yang for many fruitful discussions and their contributions. MK acknowledges support by the Deutsche Forschungsgemeinschaft (grant KO3459/1). This work was supported by the DOE under grant DE-FG02-01ER45928.

References

[1] Nitzan A and Ratner M A 2003 Electron transport in molecular wire junctions *Science* **300** 1384
[2] Agraït N, Levy Yeyati A and van Ruitenbeek J M 2003 Quantum properties of atomic-sized conductors *Phys. Rep.* **377** 81
[3] Yanson A I, Rubio Bollinger G, van den Brom H E, Agraït N and van Ruitenbeek J M 1998 Formation and manipulation of a metallic wire of single gold atoms *Nature* **395** 783
[4] Scheer E, Joyez P, Esteve D, Urbina C and Devoret M H 1997 Conduction channel transmissions of atomic-size aluminum contacts *Phys. Rev. Lett.* **78** 3535
[5] Scheer E, Agraït N, Cuevas J C, Yeyati A L, Ludolph B, Mart'in-Rodero A, Rubio-Bollinger G, van Ruitenbeek J M and Urbina C 1998 The signature of chemical valence in the electrical conduction through a single-atom contact *Nature* **394** 154
[6] Thygesen K S and Jacobsen K W 2003 Four-atom period in the conductance of monatomic al wires *Phys. Rev. Lett.* **91** 146801
[7] Ebbesen T W, Lezec H J, Hiura H, Bennett J W, Ghaemi H F and Thio T 1996 Electrical conductivity of individual carbon nanotubes *Nature* **382** 54
[8] Tans S J, Devoret M H, Dai H, Thess A, Smalley R E, Geerligs L J and Dekker C 1997 Individual single-wall carbon nanotubes as quantum wires *Nature* **386** 474
[9] Postma H W C, Teepen T, Yao Z, Grifoni M and Dekker C 2001 Carbon nanotube single-electron transistors at room temperature *Science* **293** 76
[10] Nardelli M B 1999 Electronic transport in extended systems: application to carbon nanotubes *Phys. Rev.* B **60** 7828
[11] Rosenblatt S, Yaish Y, Park J, Gore J, Sazonova V and McEuen P L 2002 High performance electrolyte-gated carbon nanotube transistors *Nano Lett.* **2** 869
[12] Lin-Chung P J and Rajagopal A K 2002 Green's function theory of electrical and thermal transport in single-wall carbon nanotubes *Phys. Rev.* B **65** 113408
[13] McEuen P L and Park J Y 2004 Electron transport in single-walled carbon nanotubes *MRS Bull.* **29** 272
[14] Ulrich J, Esrail D, Pontius W, Venkataraman L, Millar D and Doerrer L H 2006 Variability of conductance in molecular junctions *J. Phys. Chem.* **110** 2462
[15] Venkataraman L, Klare J E, Tam I W, Nuckolls C, Hybertsen M S and Steigerwald M L 2006 Single-molecule circuits with well-defined molecular conductance *Nano Lett.* **6** 458
[16] Reimers J R, Cai Z-L, Bilic A and Hush N S 2003 The appropriateness of density-functional theory for the calculation of molecular electronics properties *Ann. New York Acad. Sci.* **1006** 235–51
[17] Evers F, Weigend F and Koentopp M 2004 The conductance of molecular wires and DFT based transport calculations *Phys. Rev.* B **69** 25411
[18] Arnold A, Weigend F and Evers F 2007 Quantum chemistry calculations for molecules coupled to reservoirs: formalism, implementation, and application to benzenedithiol *J. Chem. Phys.* **126** 174101
[19] Koentopp M, Burke K and Evers F 2006 Zero-bias molecular electronics: exchange–correlation corrections to Landauer's formula *Phys. Rev.* B **73** 121403 (Rapid comm.)
[20] Sai N, Zwolak M, Vignale G and Di Ventra M 2005 Dynamical corrections to the DFT-LDA electron conductance in nanoscale systems *Phys. Rev. Lett.* **94** 186810
[21] Landauer R 1957 Spatial variation of currents and fields due to localized scatterers in metallic conduction *IBM J. Res. Dev.* **1** 223
[22] Landauer R 1970 Electrical resistance of disordered one-dimensional lattices *Phil. Mag.* **21** 172
[23] Büttiker M, Imry Y, Landauer R and Pinhas S 1985 Generalized many-channel conductance formula with application to small rings *Phys. Rev.* B **31** 6207
[24] Becke A D 1986 *J. Chem. Phys.* **84** 4524
[25] Meir Y and Wingreen N S 1992 Landauer formula for the current through an interacting electron region *Phys. Rev. Lett.* **68** 2512
[26] Xue Y Q, Datta S and Ratner M A 2002 First-principles based matrix Green's function approach to molecular electronic devices: general formalism *Chem. Phys.* **281** 151
[27] Brandbyge M, Mozos J-L, Ordejon P, Taylor J and Stokbro K 2002 Density functional method for nonequilibrium electron transport *Phys. Rev.* B **65** 165401
[28] Fisher D S and Lee P A 1981 Relation between conductivity and transmission matrix *Phys. Rev.* B **23** 6851
[29] Baranger H U and Stone A D 1989 Electrical linear-response theory in an arbitrary magnetic field: a new Fermi-surface formation *Phys. Rev.* B **40** 8169
[30] Evers F, Weigend F and Koentopp M 2003 Coherent transport through a molecular wire: DFT calculation *Physica* E **18** 255
[31] Di Ventra M, Pantelides S T and Lang N D 2000 First-principles calculation of transport properties of a molecular device *Phys. Rev. Lett.* **84** 979
[32] Di Ventra M, Pantelides S T and Lang N D 2000 The benzene molecule as a molecular resonant-tunneling transistor *Appl. Phys. Lett.* **76** 3448
[33] Di Ventra M, Pantelides S T and Lang N D 2002 Current-induced forces in molecular wires *Phys. Rev. Lett.* **88** 046801
[34] Stokbro K, Taylor J, Brandbyge M, Mosoz J-L and Ordejon P 2003 Theoretical study of the nonlinear conductance of di-thiol benzene coupled to Au(1 1 1) surfaces via thiol and thiolate bonds *Comput. Mater. Sci.* **27** 151
[35] Emberly E and Kirczenow G 2001 Comment on first-principles calculation of transport properties of a molecular device *Phys. Rev. Lett.* **87** 269701
[36] Damle P S, Ghosh A W and Datta S 2001 Unified description of molecular conduction: from molecules to metallic wires *Phys. Rev.* B **64** 201403
[37] Ke S H, Baranger H U and Yang W 2004 Electron transport through molecules: self-consistent and non-self-consistent approaches *Phys. Rev.* B **70** 085410
[38] Baer R and Neuhauser D 2003 *Ab initio* electrical conductance of a molecular wire *Int. J. Quantum Chem.* **91** 524
[39] Palacios J J 2005 Coulomb blockade in electron transport through a C_{60} molecule from first principles *Phys. Rev.* B **72** 125424

[40] Thygesen K S and Jacobsen K W 2005 Conduction mechanism in a molecular hydrogen contact *Phys. Rev. Lett.* **94** 036807

[41] Sergueev N, Roubtsov D and Guo H 2005 *Ab initio* analysis of electron–phonon coupling in molecular devices *Phys. Rev. Lett.* **95** 146803

[42] Bratkovsky A M and Kornilovitch P E 2003 Effects of gating and contact geometry on current through conjugated molecules covalently bonded to electrodes *Phys. Rev.* B **67** 115307

[43] Faleev S V, Léonard F, Stewart D A and van Schilfgaarde M 2005 *Ab initio* tight-binding LMTO method for nonequilibrium electron transport in nanosystems *Phys. Rev.* B. **71** 195422

[44] Solomon G C, Reimers J R and Hush N S 2004 Single molecule conductivity: the role of junction–orbital degeneracy in the artificially high currents predicted by *ab initio* approaches *J. Chem. Phys.* **121** 6615

[45] Garcia-Suarez V M, Kostyrko T, Bailey S, Lambert C and Bulka B R 2006 Study of transport properties of a molecular junction as a function of distance between the leads *Preprint* cond-mat/0610321 v1

[46] Grigoriev A, Sköldberg J and Wendin G 2006 Critical roles of metal–molecule contacts in electron transport through molecular-wire junctions *Phys. Rev.* B **74** 045401

[47] Kondo H, Kino H, Nara J, Ozaki T and Ohno T 2006 Contact-structure dependence of transport properties of a single organic molecule between Au electrodes *Phys. Rev.* B **73** 235323

[48] Solomon G C, Gagliardi A, Pecchia A, Frauenheim T, Di Carlo A, Reimers J R and Hush N S 2006 Molecular origins of conduction channels observed in shot-noise measurements *Nano Lett.* **6** 2431

[49] Ke S-H, Baranger H U and Yang W 2005 Contact atomic structure and electron transport through molecules *J. Chem. Phys.* **122** 074704

[50] Ke S-H, Baranger H U and Yang W 2005 Models of electrodes and contacts in molecular electronics *J. Chem. Phys.* **123** 114701

[51] Piccinin S, Gebauer R, Burke K and Car R 2008 Theoretical modeling of electronic transport in molecular devices, in preparation

[52] Frederiksen T, Brandbyge M, Lorente N and Jauho A P 2004 Inelastic scattering and local heating in atomic gold wires *Phys. Rev. Lett.* **93** 256601

[53] Chen Y-C, Zwolak M and Di Ventra M 2004 Inelastic current–voltage characteristics of atomic and molecular junctions *Nano Lett.* **4** 1709

[54] Jiang F, Zhou Y X, Chen H, Note R, Mizuseki H and Kawazoe Y 2006 First-principles study of phenyl ethylene oligomers as current-switch *Preprint* cond-mat/0601687

[55] Zhang C, Du M H, Cheng H P, Zhang X G, Roitberg A E and Krause J L 2004 Coherent electron transport through an azobenzene molecule: a light-driven molecular switch *Phys. Rev. Lett.* **92** 158301

[56] Deng W-Q, Müller R P and Goddard W A 2004 Mechanism of the Stoddart–Heath bistable rotaxane molecular switch *J. Am. Chem. Soc.* **126** 13562

[57] Kornilovitch P E, Bratkovsky A M and Williams R S 2002 Bistable molecular conductors with a field-switchable dipole group *Phys. Rev.* B **66** 245413

[58] Gosh A W, Rakshit T and Datta S 2004 Gating of a molecular transistor: electrostatic and conformational *Nano Lett.* **4** 565

[59] Xue Y and Ratner M A 2003 Microscopic study of electrical transport through individual molecules with metallic contacts. I. Band lineup, voltage drop, and high-field transport *Phys. Rev.* B **68** 115406

[60] Müller K H 2006 Effect of the atomic configuration of gold electrodes on the electrical conduction of alkanedithiol molecules *Phys. Rev.* B **73** 45403

[61] Basch H and Ratner M A 2003 Binding at molecule/gold transport interfaces. I. Geometry and bonding *J. Chem. Phys.* **119** 11926

[62] Hou S, Zhang J, Li R, Ning J, Han R, Shen Z, Zhao X, Xue Z and Wu Q 2005 First-principles calculation of the conductance of a single 4,4 bipyridine molecule *Nanotechnology* **16** 239

[63] Ke S H, Barranger H U and Yang W T 2005 Electron transport through molecules: gate-induced polarization and potential shift *Phys. Rev.* B **71** 113401

[64] Fiolhais C, Noguiera F and Marques M A L (ed) 2006 *A Primer in Density Functional Theory* 1st edn (Heidelberg: Springer)

[65] Romeike C, Wegewijs M R, Hofstetter W and Schoeller H 2006 Quantum-tunneling-induced Kondo effect in single molecular magnets *Phys. Rev. Lett.* **96** 196601

[66] Hettler M, Wegewijs M, Wenzel W and Schoeller H 2003 Current collapse in tunneling transport through benzene *Phys. Rev. Lett.* **90** 076805

[67] Hettler M and Schoeller H 2002 Nonlinear transport through a nanoscale molecule *Ann. New York Acad. Sci.* **960** 62

[68] Toher C, Filippetti A, Sanvito S and Burke K 2005 Self-interaction errors in density functional calculations of electronic transport *Phys. Rev. Lett.* **95** 146402

[69] Toher C and Sanvito S 2007 Efficient atomic self-interaction correction scheme for nonequilibrium quantum transport *Phys. Rev. Lett.* **99** 056801

[70] Delaney P and Greer J C 2004 Correlated electron transport in molecular electronics *Phys. Rev. Lett.* **93** 036805

[71] Pecchia A, Di Carlo A, Gagliardi A, Niehaus T A and Frauenheim T 2005 Atomistic simulation of the electronic transport in organic nanostructures: electron–phonon and electron–electron interactions *J. Comput. Electron.* **4** 1569

[72] Thygesen K S and Rubio A 2007 Nonequilibrium *GW* approach to quantum transport in nano-scale contacts *J. Chem. Phys.* **126** 091101

[73] van Faassen M, de Boeij P L, van Leeuwen R, Berger J A and Snijders J G 2002 Ultranonlocality in time-dependent current-density-functional theory: application to conjugated polymers *Phys. Rev. Lett.* **88** 186401

[74] Burke K, Car R and Gebauer R 2005 Density functional theory of the electrical conductivity of molecular devices *Phys. Rev. Lett.* **94** 146803

[75] Stefanucci G and Almbladh C-O 2004 Time-dependent partition-free approach in resonant tunneling systems *Phys. Rev.* B **69** 195318

[76] Stefanucci G and Almbladh C-O 2004 Time-dependent transport in fully interacting resonant tunneling systems: an exact formulation based on TDDFT *Europhys. Lett.* **67** 14

[77] Stefanucci G and Almbladh C-O 2006 An exact *ab initio* theory of quantum transport using TDDFT and nonequilibrium Green's functions *J. Phys.: Conf. Ser.* **35** 17

[78] Di Ventra M and Todorov T N 2004 Transport in nanoscale systems: the microcanonical versus grand-canonical picture *J. Phys.: Condens. Matter* **16** 8025

[79] KE S-H, Baranger H U and Yang W 2006 The dramatic role of the exchange–correlation potential in *ab initio* electron transport calculations *Preprint* cond-mat/0609637

[80] Reily Rocha A and Sanvito S 2004 Asymmetric *I–V* characteristics and magnetoresistance in magnetic point contacts *Phys. Rev.* B **70** 094406

[81] Umrigar C J and Gonze X 1993 Comparison of approximate and exact density functionals: a quantum Monte Carlo study *High Performance Computing and its Application to*

the Physical Sciences, Proc. Mardi Gras 1993 Conf. ed D A Browne *et al* (Singapore: World Scientific)
[82] Hohenberg P and Kohn W 1964 Inhomogeneous electron gas *Phys. Rev.* B **136** 864
[83] Kohn W and Sham L J 1965 Self-consistent equations including exchange and correlation effects *Phys. Rev.* A **140** 1133
[84] Perdew J P, Parr R G, Levy M and Balduz J L Jr 1982 Density-functional theory for fractional particle number: derivative discontinuities of the energy *Phys. Rev. Lett.* **49** 1691
[85] Perdew J P, Burke K and Ernzerhof M 1996 Generalized gradient approximation made simple *Phys. Rev. Lett.* **77** 3865
Perdew J P, Burke K and Ernzerhof M 1997 *Phys. Rev. Lett.* **78** 1396 (erratum)
[86] Becke A D 1993 Density-functional thermochemistry. III. The role of exact exchange *J. Chem. Phys.* **98** 5648
[87] Perdew J P, Ernzerhof M and Burke K 1996 Rationale for mixing exact exchange with density functional approximations *J. Chem. Phys.* **105** 9982
[88] Perdew J P and Zunger A 1981 Self-interaction correction to density-functional approximations for many-electron systems *Phys. Rev.* B **23** 5048
[89] Grabo T, Kreibich T, Kurth S and Gross E K U 1998 Orbital functionals in density functional theory: the optimized effective potential method *Strong Coulomb Correlations in Electronic Structure: Beyond the Local Density Approximation* ed V I Anisimov (Tokyo: Gordon and Breach)
[90] Burke K, Werschnik J and Gross E K U 2005 Time-dependent density functional theory: past, present, and future *J. Chem. Phys.* **123** 062206
[91] Runge E and Gross E K U 1984 Density-functional theory for time-dependent systems *Phys. Rev. Lett.* **52** 997
[92] Mahan G D 1990 *Many-Particle Physics* 2nd edn (New York: Plenum)
[93] Gross E K U and Kohn W 1985 Local density-functional theory of frequency-dependent linear response *Phys. Rev. Lett.* **55** 2850
Gross E K U and Kohn W 1986 *Phys. Rev. Lett.* **57** 923 (erratum)
[94] Casida M E 1996 Time-dependent density functional response theory of molecular systems: theory, computational methods, and functionals *Recent Developments and Applications in Density Functional Theory* ed J M Seminario (Amsterdam: Elsevier)
[95] Appel H, Gross E K U and Burke K 2003 Excitations in time-dependent density-functional theory *Phys. Rev. Lett.* **90** 043005
[96] van Faassen M and Burke K 2006 The quantum defect: the true measure of TDDFT results for atoms *J. Chem. Phys.* **124** 094102
[97] Drake G W F 1996 High precision calculations for helium *Atomic, Molecular, and Optical Physics Handbook* ed G W F Drake (Woodbury, NY: AIP Press) p 154
[98] Furche F and Rappoport D 2005 Density functional methods for excited states: equilibrium structure and excited spectra *Computational Photochemistry* ed M Olivucci (Amsterdam: Elsevier)
[99] Vasiliev I, Öğüt S and Chelikowsky J R 2002 First-principles density-functional calculations for optical spectra of clusters and nanocrystals *Phys. Rev.* B **65** 115416
[100] Petersilka M, Gossmann U J and Gross E K U 1996 Excitation energies from time-dependent density-functional theory *Phys. Rev. Lett.* **76** 1212
[101] Maitra N T, Zhang F, Cave R J and Burke K 2004 Double excitations in time-dependent density functional theory linear response *J. Chem. Phys.* **120** 5932
[102] Maitra N T and Tempel D G 2006 Long-range excitations in time-dependent density functional theory *J. Chem. Phys.* **125** 184111
[103] de Boeij P L, Kootstra F, Berger J A, van Leeuwen R and Snijders J G 2001 Current density functional theory for optical spectra: a polarization functional *J. Chem. Phys.* **115** 1995
[104] Vignale G and Kohn W 1996 Current-dependent exchange–correlation potential for dynamical linear response theory *Phys. Rev. Lett.* **77** 2037
[105] Marques M A L, Ullrich C, Nogueira P, Rubio A, Burke K and Gross E K U (ed) 2006 *Time-Dependent Density Functional Theory* (*Springer Lecture Notes in Physics* vol 706) (Berlin: Springer)
[106] Maitra N T, Souza I and Burke K 2003 Current-density functional theory of the response of solids *Phys. Rev.* B **68** 045109
[107] van Faassen M and de Boeij P L 2004 Excitation energies of π-conjugated oligomers within time-dependent current-density-functional theory *J. Chem. Phys.* **121** 10707
van Faassen M and de Boeij P L 2004 *J. Chem. Phys.* **121** 7035 (erratum)
[108] van Faassen M and de Boeij P L 2004 Excitation energies for a benchmark set of molecules obtained within time-dependent current-density functional theory using the Vignale–Kohn functional *J. Chem. Phys.* **120** 8353
[109] Ullrich C A and Burke K 2004 Excitation energies from time-dependent density-functional theory beyond the adiabatic approximation *J. Chem. Phys.* **121** 28
[110] Ullrich C A and Vignale G 2002 Time-dependent current-density-functional theory for the linear response of weakly disordered systems *Phys. Rev.* B **65** 245102
[111] Kamenev A and Kohn W 2001 Landauer conductance without two chemical potentials *Phys. Rev.* B **63** 155304
[112] Bokes P, Jung J and Godby R W 2006 Quantum conductance of homogeneous and inhomogeneous interacting electron systems *Preprint* cond-mat/0604317
[113] Bokes P, Jung J and Godby R W 2007 *Ab initio* formulation of the four-point conductance of interacting electronic systems *Phys. Rev.* B **76** 125433
[114] Jung J, Bokes P and Godby R W 2007 Treatment of electron viscosity in quantum conductance *Preprint* 0706.0140
[115] Prodan E and Car R 2007 DC conductance of molecular wires *Phys. Rev.* B **79** 115102
[116] van Faassen M, de Boeij P L, van Leeuwen R, Berger J A and Snijders J G 2003 Application of time-dependent current-density-functional theory to nonlocal exchange–correlation effects in polymers *J. Chem. Phys.* **118** 1044
[117] Maitra N T and Burke K 2001 Demonstration of initial-state dependence in time-dependent density functional theory *Phys. Rev.* A **63** 042501
Maitra N T and Burke K 2001 *Phys. Rev.* A **64** 039901 (erratum)
[118] Kohn W and Luttinger J M 1957 Quantum theory of electrical transport phenomena *Phys. Rev.* **108** 590
[119] Cohen-Tannoudji C, Dupont-Roc J and Grynberg G 1992 *Atom–photon Interactions: Basic Processes and Applications* (New York: Wiley)

[120] Gebauer R, Piccinin S and Car R 2005 Quantum collision current in electronic circuits *ChemPhysChem* **6** 1727
[121] Piccinin S 2006 Theoretical modeling of electronic transport in molecular devices *PhD Thesis* Princeton University
[122] Stefanucci G, Kurth S, Gross E K U and Rubio A 2007 Time-dependent transport phenomena *Molecular Electronics: Analysis, Design, and Simulation* (*Elsevier Series on Theoretical Computational Chemistry* 17) ed J Seminario pp 247–84
[123] Kurth S, Stefanucci G, Almbladh C-O, Rubio A and Gross E K U 2005 Time-dependent quantum transport: a practical scheme using density functional theory *Phys. Rev.* B **72** 035308
[124] Stefanucci G 2007 Bound states in *ab initio* approaches to quantum transport: a time-dependent formulation *Phys. Rev.* B **75** 1195115
[125] Verdozzi C, Stefanucci G and Almbladh C-O 2006 Classical nuclear motion in quantum transport *Phys. Rev. Lett.* **97** 046603